Induced pluripotent stem cell derived macrophages to model Niemann-Pick disease Type C

Mariana Marques Baltazar
Master's degree in Applications in Biotechnology and Synthetic Biology
Department of Chemistry and Biochemistry and Department of Biology
2021-2022

Mentor
Yunus Alpagu PhD, Director of R&D Cellular Models, Centogene GmbH

Supervisor
Artur Rodrigues MSc, Research Associate at R&D Cellular Models, Centogene GmbH

Co-mentor
Vasco Almeida PhD, Senior Professor, Faculty of Sciences of University of Porto

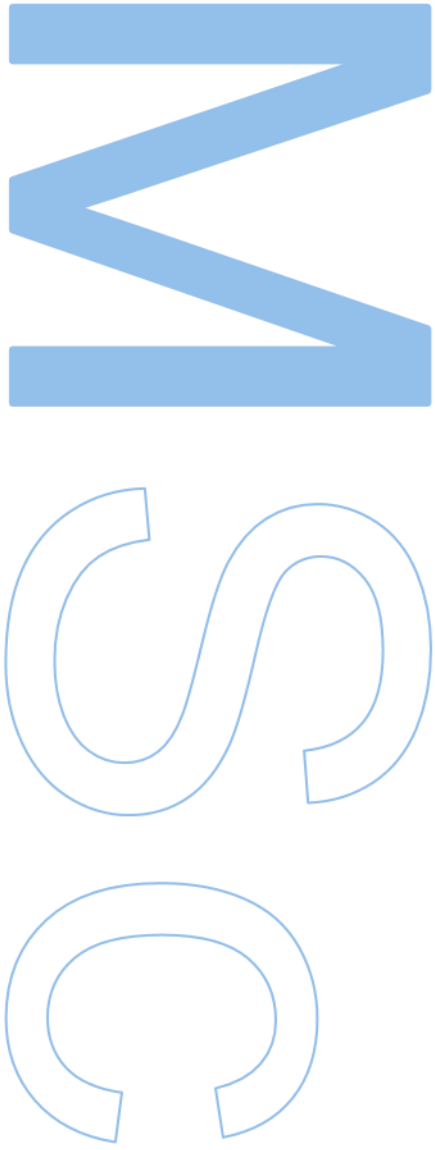


CENTOGENE
THE RARE DISEASE COMPANY

U.PORTO
FACULDADE DE CIÊNCIAS
UNIVERSIDADE DO PORTO

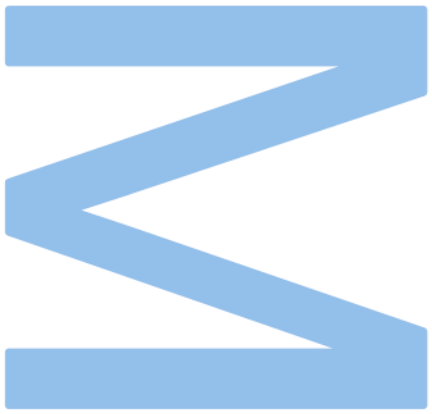

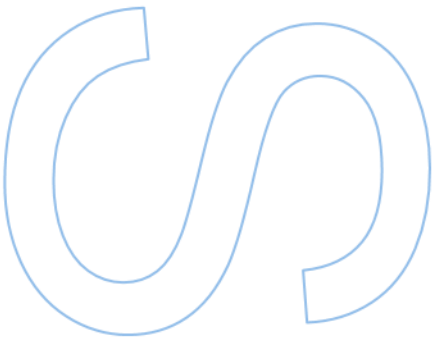

Nothing in life is to be feared, it is only to be understood. Now is the time to understand more, so that we may fear less.

Marie Curie

Sworn Statement

I, Mariana Marques Baltazar, enrolled in the Master's degree Applications in Biotechnology and Synthetic Biology at the Faculty of Sciences of the University of Porto hereby declare, in accordance with the provisions of paragraph a) of Article 14 of the Code of Ethical Conduct of the University of Porto, that the content of this internship report reflects perspectives, research work and my own interpretations at the time of its submission.

By submitting this internship report, I also declare that it contains the results of my own research work and contributions that have not been previously submitted to this or any other institution.

I further declare that all references to other authors fully comply with the rules of attribution and are referenced in the text by citation and identified in the bibliographic references section. This internship report does not include any content whose reproduction is protected by copyright laws.

I am aware that the practice of plagiarism and self-plagiarism constitute a form of academic offense.

Mariana Marques Baltazar

29.09.2022

Acknowledgements

Acknowledgements

First, I would like to thank Dr. Yunus Alpagu for sharing his knowledge and giving me the opportunity to do an in internship at his department. Secondly, I would like to thank my supervisor Artur Rodrigues for his openness and patience in guiding me throughout this internship, always available to help and give constructive criticism. I would also like to thank the rest of the team for sharing their knowledge with me and creating an amazing working environment.

To my mentor at FCUP, Professor Vasco Almeida, I would like to thank for always being available and for his advice.

Lastly, I would like to express my gratitude to my family who supported and encouraged me all these years, especially during this internship from far away and to my friends for putting up with me during this journey and for always being able to lift me up.

Resumo

Resumo

A doença de Niemann-Pick tipo C (NPCD) é uma doença rara de armazenamento lisosomal causada por mutações nos genes NPC1 (prevalência de 95%) ou NPC2 (prevalência de 5%) levando à acumulação de colesterol não esterificado em lisosomas e endosomas tardios, tal como, metabolismo de esfingolípidos e autofagia afetados. É uma doença neurovisceral principalmente com inicio na infância caracterizada por ataxia cerebelar, disfagia, paralisia vertical supranuclear, entre outros, com possível hepato- e esplenomegalia, culminando numa doença neurológica fatal. Até à data, não existe uma terapia eficaz para o tratamento da NPCD, o que exige mais investigação na doença.

Em resposta à falta de modelos *in vitro* biologicamente relevantes, este trabalho caracteriza um novo modelo de macrófagos derivados de *induced pluripotent stem cells* (iMph) de NPCD, para fornecer uma nova plataforma para estudar a doença e acelerar a descoberta de novas terapias.

Neste trabalho, citometria de fluxo, microscopia de fluorescência de *high-throughput* e sequenciamento de RNA foram utilizados para caracterizar o modelo celular e o fenótipo da doença. Os macrófagos gerados *in vitro* apresentam os marcadores CD14, CD45, CD68, CD163 e CD86, capacidade fagocitária, bem como potencial de polarização em M1 e M2 confirmando a sua funcionalidade para modelar macrófagos de forma fiável. Fenotípicamente encontramos baixo sinal de proteína NPC1 juntamente com acumulação de colesterol não esterificado com aparente localização lisossomal em iMph derivados de paciente, confirmando o fenótipo NPCD. Também observámos uma ligação entre o estado de polarização de iMph e a assinatura transcripcional de NPCD, uma vez que M2 iMph apresentaram consideravelmente mais genes diferencialmente expressos do que M1 iMph, indicando que o estado de polarização pode ser um factor importante a considerar ao estudar a doença.

Em suma, caracterizámos com sucesso tanto o modelo *in vitro* de macrófagos como as características-chave da doença, constituindo um modelo celular novo e robusto e, esperamos, a longo prazo, desvendar novas e melhores terapias para os doentes com NPCD.

Palavras-chave: Doença de Niemann-Pick tipo C, NPC1, doenças de armazenamento lisossomal, modelo de doença, macrófagos derivados de células estaminais pluripotentes induzidas.

Abstract

Abstract

Niemann-Pick disease type C (NPCD) is a rare lysosomal storage disease caused by mutations in NPC1 (95% prevalence) or NPC2 (5% prevalence) genes leading to lysosomal and late endosomal accumulation of unesterified cholesterol, impaired sphingolipid metabolism and autophagy. It is a neurovisceral disease with mainly an infantile onset characterized by cerebellar ataxia, dysphagia, vertical supranuclear gaze palsy, among others, with possible hepato- and splenomegaly, culminating in a fatal neurological disease. To date, no effective therapy is available for the treatment of NPCD, which calls for further research in the field.

In response to the lack of biologically relevant *in vitro* models, this work characterizes a novel induced pluripotent stem cell (iPSC) derived macrophage (iMph) disease model of NPCD to provide a new platform to further study and accelerate drug discovery.

Here we use flow cytometry, high-throughput fluorescence microscopy and RNA sequencing to characterize the model system and disease phenotype. The *in vitro* generated macrophages presented signature markers CD14, CD45, CD68, CD163 and CD86, phagocytic capability as well as polarization potential into M1 and M2 confirming their functionality to reliably model macrophages. Phenotypically we found low signal of NPC1 protein along with unesterified cholesterol accumulation with apparent lysosomal localization in patient iMph, confirming NPCD phenotype. We also observed a connection between the polarization status of iMph and the transcriptional signature of NPC1 as M2 presented considerably more DEGs than M1, indicating that the polarization status might be an important factor to consider when studying the disease.

Overall, we have successfully characterized both the *in vitro* macrophage model system and key characteristics of NPCD disease, depicting a novel and robust disease model for the disease and, hopefully, in the long run unravel new and better therapies for NPCD patients

Keywords: Niemann-Pick disease type C, NPC1, lysosomal storage diseases, disease modelling, induced pluripotent stem cell derived macrophages

Table of Contents

Table of Contents

List of Tables

List of Figures

List of Abbreviations

2D – Two-dimensional

3D – Three-dimensional

AKT – Protein Kinase B

B-CD – 2-hydroxypropyl-β-cyclodextrin

bFGF – Basic fibroblast growth factor

BMP4 – Bone morphogenetic protein 4

CCL – Chemokine (C-C motif) ligand

CD – Cluster of Differentiation

CDH1 – Cadherin 1

CNS – Central Nervous System

CXCL – Chemokine (C-X-C motif) ligand

CXCR – C-X-C chemokine receptor

DCX – Doublecortin

DEG – Differentially expressed genes

DNA – Deoxyribonucleic acid

DPBS – Dulbecco's phosphate-buffered saline

EB – Embryoid Body

EDTA – Ethylenediaminetetraacetic acid

EMA – European Medicines Agency

ER – Endoplasmic Reticulum

ESC – Embryonic stem cell

FBS – Fetal Bovine Serum

FC – Fold Change

FDA – Food and Drug Administration

FDR – False discovery rate

Flt3 – Fms Related Receptor Tyrosine Kinase 3

FSC – Forward scatter

GATA – GATA Binding Protein

GFAP – Glial fibrillary acidic protein

GM-CSF – Granulocyte-macrophage colony-stimulating factor

HES5 – Hes Family BHLH Transcription Factor-5

HPC – Hematopoietic progenitors

HT – high throughput

IC – Immune complexes

IFNGR – Interferon gamma receptor

IFN-γ – Interferon gamma

IGF2 – Insulin-like growth factor 2

IL – Interleukin

iMph – induced pluripotent stem cell macrophage

IPA – Ingenuity Pathway Analysis

iPSC – Induced pluripotent stem cell

JAK – Janus kinase

KLF4 – Krüppel-like factor 4

LAMP – Lysosomal associated membrane proteins

LC3BII – Microtubule associated protein 1 light chain 3 beta

LDL – Low density lipoprotein

LDLR – Low density lipoprotein receptor

LE – Late endosome

LPS – Lipopolysaccharide

LSD – Lysosomal Storage Disease

LY – Lysosome

M-CSF – Macrophage colony-stimulating factor

MHCII – Major histocompatibility complex class II

mRNA – Messenger ribonucleic acid

NFkB – Nuclear factor kappa-light-chain-enhancer of activated B cells

NGS – Next Generation Sequencig

NO – Nitric Oxide

NPC1 – Niemann-Pick C1

NPC2 – Niemann-Pick C2

NPCD – Niemann-Pick disease Type C

NTD – N-Terminal domain

OCT4 – Octamer-binding transcription factor 4

PAMP – Pathogen-associated molecular patterns

PAX6 – Paired Box 6

PCA – Principal component analysis

PCSK9 – Proprotein Convertase Subtilisin/Kexin Type 9

PFA – Paraformaldehyde

PTC – Premature stop codon

qPCR – Real time polymerase chain reaction

R&D – Research and development

RD – Rare disease

RNA – Ribonucleic acid

ROI – Reactive oxygen intermediates

RT – Room temperature

S1P – Sphingosine-1-Posphate

SCF – Stem cell factor

SE – Standard Error

SEM – Standard Error of the Mean

SGMS – Sphingomyelin Synthase

SGPP – Sphingosine-1-phosphate phosphatase

SM – Small Molecules

SOCS1 – Suppressor of cytokine signalling 1

SOX2 – sex determining region Y-box 2

SP – Sphingosine

SPHK – Sphingosine kinase

SSC – Side scatter

SSD – Sterol sensing domain

SSEA – Stage-specific embryonic antigen

STAT – Signal transducer and activator of transcription

STR – Short tandem repeat

TGF-β – Transforming growth factor beta

Th – T helper

TLR – Toll-like receptor

TNF-α – Tumor necrosis factor alpha

TPO – Thyroid Peroxidase

VEGF – Vascular endothelial growth factor

Chapter 1
Introduction

1. Introduction

1.1. Rare Diseases

Rare diseases (RD) are medical conditions that affect a small percentage of the general population. There is no agreed upon definition to characterize a rare disease, and, as such, it is usually linked to the point prevalence of the disease and is based on a threshold prevalence (Nguengang Wakap et al., 2020). In Europe, a disease is considered rare if it affects 1 person in every 2 000, hence, it is estimated that there are about 300 million rare disease patients and between 6 000 and 7 000 rare diseases worldwide (Orphanet: About Orphanet, n.d.; Orphanet: About Rare Diseases, n.d.).

RDs, in their nature, are largely chronic degenerative diseases with a genetic origin (~80%) and a childhood onset (~70%) meaning that many of their patients do not reach adulthood (Rare diseases, n.d.; Nguengang Wakap et al., 2020). The vast majority of these diseases have no treatment, and the few that do exist are unsatisfactory and/or very costly. Aiming to prevent overlooking these patients, the European Union and other parts of the world made RDs a public health priority, providing financial support for the health and biotech industries to stimulate research and promote the development of orphan drugs (Rare diseases, n.d.; Pogue et al., 2017).

1.1.1. The role of CENTOGENE

In this context, Centogene was founded in 2006 aiming to accurately diagnose, understand and treat rare genetic, metabolic and neurodegenerative diseases (About Us: The CENTOGENE Story, n.d.). To date, Centogene has diagnosed more than 2 500 rare diseases worldwide, and has amassed one of the broadest portfolios of genetic diagnostic tests, covering more than 19 000 genes, contributing to accurate and accelerated diagnosis (About Us: The CENTOGENE Story: Centogene.Com, n.d.). From the beginning Centogene has been data-driven, which enabled them to create a massive Bio/Databank, “the world’s largest real-world data repository for rare and neurodegenerative diseases”(The CENTOGENE Biodatabank, n.d.) , which constitutes it's biggest asset and what distinguishes Centogene from its peers. The Bio/Databank provides extremely valuable knowledge to continually develop and deliver excellence in its diagnostic capabilities, as well as help elucidate disease pathways and accelerate

drug discovery with the help of in-house research teams and multiple collaborations with pharma and biotech companies. As a result, Centogene settled on a mission to “enable the cure of 100 rare diseases in 10 years”(About Us: The CENTOGENE Story n.d.) and, at the moment, the company focuses on lysosomal storage diseases, these being, Gaucher disease, genetic Parkinson and Niemann-Pick type C (About Us: The CENTOGENE Story n.d.).The latter will be the focus of this report.

1.2. Niemann-Pick Disease Type C

Niemann-Pick disease type C (NPCD) is estimated to affect around 1 person per 100 000. It’s part of a group of diseases known as lysosomal storage diseases (LSD), which comprises over 70 monogenic diseases, being its vast majority autosomal recessive, which influence the proper functioning of the lysosomal catabolism, leading to lysosomal dysfunction (Platt et al., 2018). NPCD can be caused by mutations in either Niemann-Pick C1 (NPC1) gene (prevalence of 95% with 549 known mutations) or Niemann-Pick C2 (NPC2) gene (prevalence of 5% with 29 known mutations), resulting in protein misfolding, proteasomal degradation and hindered trafficking, depending on the localization of the mutation. This leads to abnormal intracellular transport of endocytosed cholesterol and glycosphingolipids, resulting in sequestration of these lipids in lysosomes and late endosomes, being the accumulation of intracellular unesterified cholesterol one of the main hallmarks of the disease (Vanier, 2010; Völkner et al., 2021).

1.2.1. Clinical manifestations

From a clinical point of view, NPCD presents heterogenous clinical manifestations, not only when it comes to the involvement of multiple organs but also to the age of disease onset, ranging from perinatal to adulthood (Vanier, 2013).

NPCD is considered a neurovisceral disease, characterized by neurological and/or psychiatric manifestations as well as visceral involvement of liver and spleen (hepatomegaly and splenomegaly, respectively) (Vanier, 2013; Pallottini and Pfrieger, 2020). Neurologically, patients of more than one age group typically present cerebellar ataxia, progressive dementia, dysphagia, and vertical supranuclear gaze palsy (Vanier, 2013). The majority of NPCD patients present an infantile onset mainly represented by a delay in motor milestones with potential to thrive into early adulthood (Ordoñez &

Steele, 2017). Another large group of patients presents a juvenile form with cognitive impairment, ataxia, and dystonia (Pallottini and Pfrieger, 2020). As for the adult form, patients usually present cognitive impairment and psychiatric symptoms such as dementia (Vanier, 2013; Pallottini and Pfrieger, 2020).

A small group of patients die within the first few months of life due to hepatic or respiratory failure. In other cases, the progression of the disease eventually culminates in progressive and ultimately fatal neurological disease (Vanier, 2013). The figure 1 represents an overview of NPCD clinical manifestations according to the age of onset.

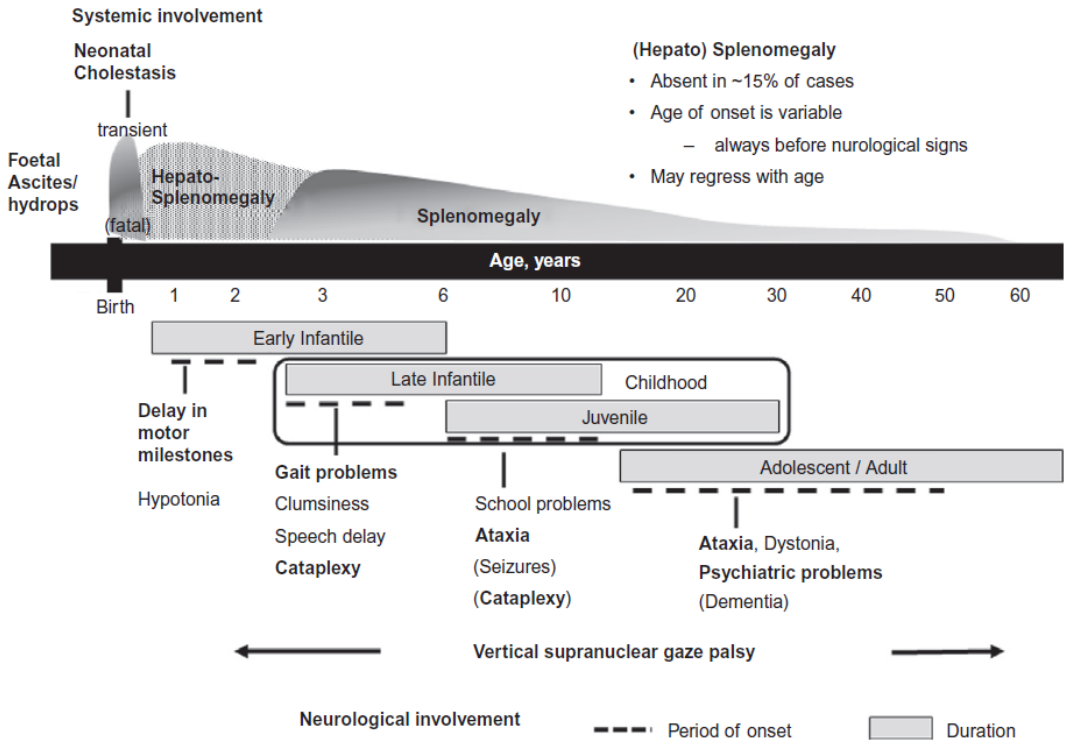

Figure 1- Schematic overview of the clinical manifestations of NPC1, with a classification based on the main initial neurological manifestations (Vanier, 2013).

1.2.2. Diagnosis

To make a diagnosis, an initial clinical assessment should be performed, checking for the most common symptoms. Due to the great heterogeneity in the clinical manifestations of the disease, if NPCD is suspected, a laboratory diagnosis combining biochemical and molecular techniques is recommended for confirmation (Vanier, 2010, 2013; Geberhiwot et al., 2018). Histopathological examination such as bone morrow or

liver biopsies can be useful to identify the presence of foamy cells, a phenotype that will be discussed further in the text (Sitarska & Ługowska, 2019; Vanier, 2010).

Since one of the main hallmarks of the disease is the accumulation of cholesterol, filipin, a polyene antibiotic with affinity for unesterified cholesterol is used to infer such accumulation. Filipin forms a highly fluorescent complex, allowing free cholesterol to be visualized by fluorescence microscopy (Vanier & Latour, 2015). In patients, the procedure is based on a skin biopsy followed by fibroblasts cultured in low density lipoprotein (LDL) enriched medium. Staining is then carried out in fixed cells, since filipin disrupts the bilayer membrane structure, revealing numerous fluorescing perinuclear vesicles reflective of the intracellular cholesterol accumulation, a pattern observed in 80% to 85% of NPCD cases (Sitarska & Ługowska, 2019; Vanier, 2010; Vanier & Latour, 2015).

Filipin test was once the gold standard in diagnosing NPCD but the lack of standardization between protocols and the existence of a range of variations in the filipin pattern makes it less ideal than desired (Sitarska and Ługowska, 2019).This leads to an increase in the importance of genetic diagnostic methods that, coupled with technological development, made genetic testing not only faster and more reliable, but also cheaper.

Accordingly, nowadays the first line of diagnosis involves testing suspected NPCD patients for biomarkers and subsequently genetically sequencing NPC1 and NPC2 genes or, alternatively, diagnosing genetically as a first line, followed by confirmation by other genomic methods (Patterson et al., 2017). At the moment the main biomarkers available are Oxysterols such as Cholestane-3b,5a,6b-triol (C-triol) and 7-ketocholesterol (7-KC) and lysosphingolipids such as Lysosphingomyelin-509 (Lyso-SM-509) and Lysosphingomyelin, which have the advantage of being non-invasive, scalable and low cost compared to the standard filipin test (Patterson et al., 2017).

Ultimately, genetic testing is the most sensitive method and is used to confirm the diagnosis. Sequencing can be done by Sanger sequencing and, more recently, NGS (next generation sequencing) has been progressively adopted. Given the polymorphic nature of NPC1, a negative or heterozygous result must be further confirmed by other genetic methods such as array comparative genomic hybridization (Patterson et al., 2017; Vanier, 2010).

1.2.3. Pathophysiology of Niemann-Pick Disease Type C

1.2.3.1. Niemann-Pick Type C1 protein structure and function

The NPC1 gene encodes for a membrane glycoprotein localized mostly in the late endosome (LE) and lysosomes (LY) with 1278 residues (Yu et al., 2014). It has 13 helix transmembrane domains, 3 large loops that project into the lumen of the LE or LY four small luminal loops, six small cytoplasmic loops, and finally a cytoplasmic tail. The latter constitutes a di-leucine motif that is thought to promote the trafficking of NPC1 to the endosomal compartment after its production in the endoplasmic reticulum and passage through the Golgi apparatus (Li et al., 2016; Yu et al., 2014).

The region from the 3rd to the 7th transmembrane domain is called the "sterol-sensing domain" (SSD), this is a region conserved between species and is thought to play an important regulatory role in their response to cholesterol (Yu et al., 2014). It has a two-way cavity open to the endosomal lumen and a luminal leaflet of the lipid bilayer that may explain how cholesterol is transported by NPC1 across the bilayer (Li et al., 2016).

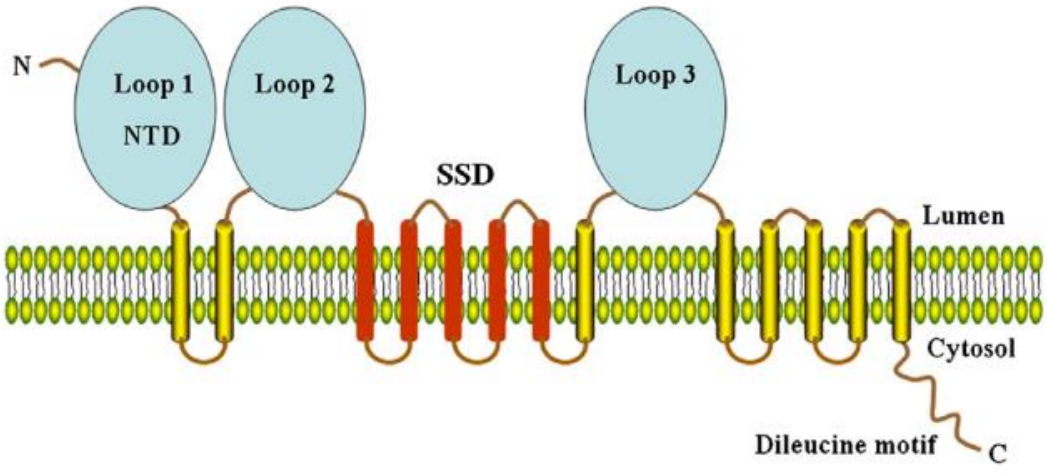

Figure 2- Schematic NPC1 protein structure (Yu et al., 2014).

Although the essential role of NPC1 for the efflux of cholesterol into late endosomes and lysosomes is clear, many of the functions of this protein and its exact mechanism of action *in vivo* remains to be elucidated.

1.2.3.2. Lipid dysregulation

In the mammalian cell, cholesterol is an essential component of the cell membrane and can be acquired in two ways, by *de novo* synthesis in the endoplasmic reticulum (ER) and by internalization through receptor mediated endocytosis of LDL (Ikonen & Zhou, 2021; Yu et al., 2014). In a normal physiological condition, LDL is endocytosed and transported to LE and LY where undergoes hydrolysis by an acid lipase, freeing the cholesterol. Then, according to the "Handoff" model, free cholesterol binds to NPC2 in LE/LY with its hydroxyl group exposed and is transferred to N-terminal domain (NTD) of NPC1. From there, free cholesterol is transported out of the vesicles and delivered to other cell compartments (Li et al., 2016; Nadjar & Vanier, 2018; Yu et al., 2014).

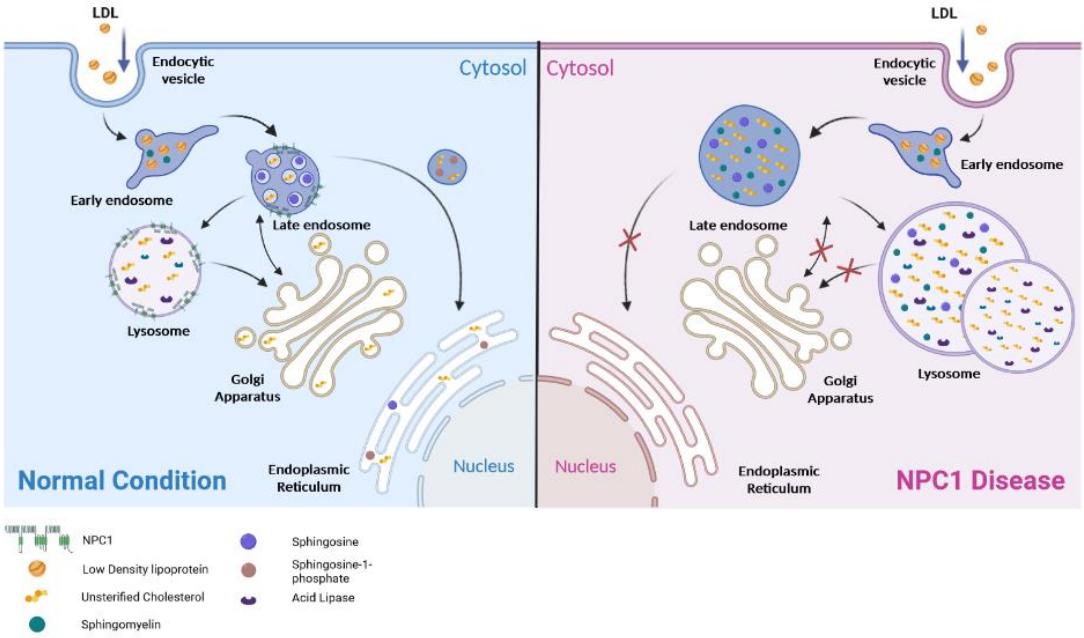

Figure 3- Brief overview of main pathophysiological pathway in NPC1. The mutation in NPC1 prevents release of unesterified cholesterol and sphingolipids from LE/LY resulting in scarcity in the receiving organelles such as ER and Golgi apparatus, leading to enlarged lysosomes. Created in BioRender.com.

Disruption of NPC1 protein results in accumulation of unesterified cholesterol in LE/LY, since it blocks cholesterol transport to other cell compartments. Sequestration of unesterified cholesterol in LE/LY is not detected by the ER so homeostatic mechanisms are not initiated, which leads to a continuous accumulation of cholesterol culminating in, for example, the formation of foam cells, lipid-laden macrophages (Pacheco &

Lieberman, 2008; Tang et al., 2010). Regarding the brain, there is accumulation mainly of glycosphingolipids, such as GM3 and GM2, and to a lesser extent of cholesterol. This can be due to the fact that, cholesterol is mainly obtained by *de novo* synthesis, for endogenous use or trafficking to the remaining cells of the nervous system, due to its inability to cross the blood-brain barrier not allowing uptake of cholesterol from other regions of the body (Tang et al., 2010).

The arrest of cholesterol in LE/LY has two main consequences. On one hand, there is accumulation of cholesterol and other lipids intracellularly resulting in cholesterol scarcity in the receiving organelles, which can greatly affect key cellular processes. On the other hand, a decrease in available free cholesterol leads to a decrease in oxysterols and thus absence of negative feedback in the de novo synthesis of cholesterol. This can lead to an exacerbation in cholesterol production and consequently an increase in cholesterol accumulation, resulting in a vicious circle (Pacheco & Lieberman, 2008).

Furthermore, it appears that lipid metabolism as a whole is impaired. Other lipids such as sphingosine and sphingomyelin are elevated in NPCD patients (Pacheco & Lieberman, 2008; Wheeler & Sillence, 2020). Indeed, the only approved specific therapy, Miglustat, is a glucosylceramide synthase inhibitor that decreases glycosphingolipid accumulation. Patients undergoing Miglustat treatment show a delay in neurological symptoms indicating increased life expectancy (Pineda et al., 2018). However, it does not lead to a reduction in intracellular cholesterol, which for instance, when tested for disruption of cholesterol uptake and thus reduction of cholesterol, improvements at the neurological level were not reported, only at the visceral level. This may indicate that cholesterol accumulation is not the direct cause of neurodegeneration in NPCD (Newton et al., 2018).

1.2.3.3. Endocytosis and autophagy dysregulation

Other cellular processes appear to be affected in NPCD. Endocytosis, the process by which the cell internalizes substances and renews the outer membranes, appears to be compromised in NPCD (Wheeler & Sillence, 2020). The permanent high concentration of cholesterol in LE/LY blocks dynein from dissociating with the organelles, remaining immobilized and hinder its fusion with early endosomes. Likewise, the annexin A2 and A6 proteins do not dissociate from the organelles and, therefore, are not replenished to continue the endocytic process (Wheeler & Sillence, 2020).

Given this slowing in the endocytic process and in view of the direct relationship between autophagy and lipid metabolism (macrolipophagy), it is to be expected that autophagy, the process by which the cell processes damaged or old macromolecules and organelles, is also affected (Singh et al., 2009). In general, increased intracellular lipids affect autophagic clearance and, in NPCD, an exacerbated autophagic stress due to reduced autolysosome clearance is observed (Wheeler & Sillence, 2020).

Liedtke et al (2022) reported an increase in microtubule associated protein 1 light chain 3 beta (LC3BII) levels indicating an increase in autophagosomes which is in line with previous findings of its accumulation due to defective clearance, as well as hampered expression of p62 and impaired fusion of autophagosomes and lysosomes which can further explain increased LC3BII levels (Liedtke et al., 2022). In short, NPCD presents defective autophagy leading to autophagic stress which in turn can cause cellular stress and death.

During LDL uptake through endocytosis, these vesicles are highly rich in sphingolipids which need to be recycled or transported to the lysosome for degradation (Newton et al., 2018; Wheeler and Sillence, 2020). With the endocytic pathway being impaired, it is possible that it has a major impact on sphingolipid accumulation.

In sum, there is impairment in lipid trafficking leading to accumulation of cholesterol, sphingolipids and complex gangliosides in various cell types, affecting other basal cell processes such as autophagy and endocytosis that may ultimately compromise cell viability.

1.2.4. Therapies in Niemann-Pick Disease Type C

Currently, NPCD does not have a cure and as previously mentioned, up until now, only one therapy has been approved, Miglustat (Miglustat Gen.Orph | European Medicines Agency, n.d.).

Other therapies are being developed. Cyclodextrins seem very promising as they have the ability to move deposits of lipids and seem to ameliorate the intracellular cholesterol accumulation (Matencio et al., 2020). 2-Hydroxypropyl-β-cyclodextrin (B-CD), has shown to reverse NPC1 deficiency by sequestrating stored cholesterol and increase its ER availability in mice (Peake and Vance, 2012). Similarly, 2-Hydroxypropyl-γ-cyclodextrin has shown to relieve the accumulation of cholesterol in disease fibroblast,

increase its ER availability and improve autophagic activity while simultaneously tackling a major problem related to B-CD, ototoxicity (Matencio et al., 2020; Singhal et al., 2020). However, cyclodextrins have a big difficulty in crossing the blood brain barrier, therefore, derivatives such as polymers are being developed in hope to tackle this issue, as it is very important to treat the disease in a neurological level (Matencio et al., 2020).

Arimoclomol, a small molecule able to cross the blood brain barrier, activates the heat shock response, a cellular mechanism which helps in proper protein folding and promotes lysosomal homeostasis, has been approved by European Medicines Agency (EMA) and Food and Drugs Agency (FDA) as a potential drug for NPCD treatment and is currently under clinical trial showing a significant reducing in disease progression (Matencio et al., 2020; Mengel et al., 2021). Ultimately, therapy is scarce and only slightly slows the progression of the disease. This calls for a desperate need for new and more effectives therapies.

In drug discovery, the translation of drug candidates from preclinical and animal studies into clinical success is very low, despite increasing and substantial investments in areas such as neurodegeneration (Horvath et al., 2016).

In part, cellular models highly contribute for the validation and screening of new compounds. However, the majority of currently used cellular models have been established a long time ago in immortalized cell lines that can have little to no disease relevance. Therefore, the lack of appropriate disease models contributes to the low success rates of preclinical (Horvath et al., 2016).

Overall, there is a need to develop more phenotypically relevant disease models that allow us to do proper compound screenings and validation in order to increase the success rate, which translates into a reduction in the investment needed to bring a drug to the market. This is of extreme relevance when it comes to orphan drugs for rare diseases where the market is small with low investment return (Fonseca et al., 2019; Horvath et al., 2016; Ordoñez & Steele, 2017).

1.2.5. Disease Models in Niemann-Pick Disease Type C

In recent decades, NPCD has been acquiring increasingly more disease models that go from mice to zebrafish. Although, such advance in *in vivo* modelling allowed the understanding of many aspects of disease pathophysiology, the applicability of such models for drug screening and validation is a key point to be considered.

The most used disease models for NPCD are mice, for *in vivo* studies, and fibroblast cell cultures for *in vitro* studies, as they are highly proliferative and rather easily obtainable. With new technologies, there has been a paradigm shift and newer, more disease relevant models have been developed (Völkner, Liedtke, Hermann, et al., 2021).

As with other diseases, the first mouse models resulted from spontaneous mutations. NPC1^{nih} mice was derived from an insertion of a retrotransposon in the nih allele in BALB/c strain and NPC1^{spm} resulted from an insertion in C57BL/Ks strain, both resulting in NPC1 null allele and complete knock-out (Pallottini & Pfrieger, 2020; Völkner, Liedtke, Hermann, et al., 2021). They present clinical similarities, progressive weight loss and motor coordination loss, tremor, ataxia with premature death. Furthermore, NPC1^{nih} presented free cholesterol and gangliosides accumulation, demyelination, gliosis and other neurological alterations and, NPC1^{spm} likewise, presented sphingomyelin accumulation and impaired sphingomyelinase activity (Pallottini & Pfrieger, 2020; Völkner, Liedtke, Hermann, et al., 2021). These mice models are still some of the most used models in NPCD and show clinically and biochemically relevant and comparable characteristics to humans. However, it should be noted that a complete protein knock-out is rare and most mutations in humans lead to dysfunctional and misfolded proteins (Pallottini & Pfrieger, 2020). Additionally, animal experimentation carries a lot of ethical responsibility along with long and costly experiments with the impossibility to perform high-throughput techniques such as drug screenings (Völkner, Liedtke, Hermann, et al., 2021).

Regarding cellular models, immortalized and CHO cells lines were early on established, being CHO cells a powerhouse behind biological knowledge of the disease (Pallottini and Pfrieger, 2020). However, the caveats associated with the use of cell lines are currently well known, with major genetic and epigenetic abnormalities and overtime identity loss being some of the aspects compromising its reliability (Horvath et al., 2016).

Followed, as technology evolved, and given the neurovisceral nature of the disease, models of central nervous system (CNS) cell types originated from mice were

developed. They revealed unique characteristics of these cells such as impaired synaptic function, cholesterol accumulation, and cholesterol loss in axons, demonstrating the importance of using relevant models of the disease. In addition, immune cells such as B cells, invariant Natural Killer T cells and macrophages have been used and to a lesser extent hepatocytes and splenocytes were used despite being relevant to the disease (Pallottini & Pfrieger, 2020). Yet these models are derived from other organisms. This is due to the great difficulty in obtaining primary cell cultures from humans, due to the inability to source cells in large quantities as certain tissues are practically impossible to reach such as the brain (Völkner, Liedtke, Hermann, et al., 2021).

The development of induced pluripotent stem cells came to answer this problem and revolutionize disease cellular models.

1.3. Induced pluripotent stem cells

In 2006, induced pluripotent stem cells (iPSCs) were presented at the International Society for Stem Cell Research meeting in Toronto, Ontario and the field of cellular reprogramming was revolutionized (Lensch & Mummery, 2013; G. Liu et al., 2020). iPCS are adult somatic cells reprogrammed with four transcription factors to regain pluripotency. This technology impacted multiple fields of research such as cardiac diseases and neurological disorders, and stem cell research had a tremendous boom in interest and has shown great promise in regenerative medicine, disease modeling and drug discovery screenings (G. Liu et al., 2020).

Due to the importance of this technology and its impact in various fields of research and in the way research itself is carried out, in 2012, both authors Shinya Yamanaka (Kyoto University, Japan and Gladstone Institutes, USA) and John Gurdon (Gurdon Institute, Cambridge, UK) were co-recipients of the Nobel Prize for Physiology or Medicine for their discovery that mature cells could be reprogrammed into a pluripotent state (Liu et al., 2020).

The reprogramming of somatic cells into iPSCs, follows a general process. Somatic cells are transduced with a combination of transcription factors that promote staminality, being the original ones, octamer-binding transcription factor 4 (OCT4) , sex determining region Y-box 2 (SOX2), Krüppel-like factor 4 (KLF4) and c-Myc (Karagiannis et al., 2019). The whole process is taken ahead on feeder cells or equivalent feeder free

and xeno-free systems, then these can be differentiated into a multitude of cell models, 2D and 3D, as well as used for drug screenings, developmental studies and so on (Karagiannis et al., 2019). A brief scheme of the method can be found in figure 4.

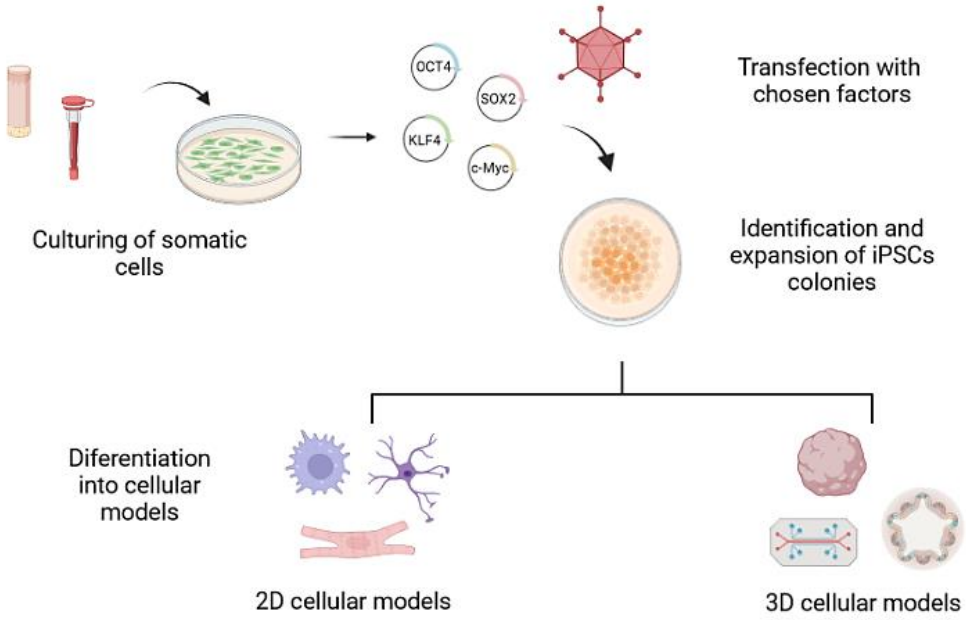

Figure 4- Schematic illustration of the general process of iPSCs generation. *C*reated in BioRender.com.

Unfortunately, the method proved to have low efficiency with only a small proportion of cells undergoing reprogramming as well as they presented some genetic differences from ESCs cells, which led the scientific community to optimize and develop alternative methods by using different cell types, combinations of reprogramming factors and delivery methods (Karagiannis et al., 2019; Zhang et al., 2020).

Starting with cell types, to date, numerous cell types from various common research species such as human, mice, pig, monkey, rabbit among others have been successfully reprogrammed which indicates that all cells in the body seem to be possess the ability to become iPSCs, however at different efficiency rates and require different delivery methods (Karagiannis et al., 2019).

Originally murine fibroblasts were used, therefore the first trials in reprogramming human cells were also fibroblasts, however due to the need to perform a skin biopsy, which is an evasive procedure and requires medical expertise to perform, other cell types were desired (Karagiannis et al., 2019). A promising and desirable source of cells would be peripheral blood cells, as a simple blood sample would allow to obtain various cell

types and indeed, iPSCs from T cells, B cells, fibrocytes and others were successfully reprogrammed (Karagiannis et al., 2019).

The reprogramming process depends on the transient expression of exogenous transcription factors to allow cell to initiate the reprogramming and complete it. The delivery method highly impacts the efficiency of the reprogramming as well (Karagiannis et al., 2019).

Regarding delivery methods, according to the purpose of the iPSCs different methods will be more suitable. Retro/lentiviruses and adenoviruses are very easy and accessible methods, being Retro/lentiviruses the most efficient and therefore one of the methods of choice for research purposes. On the other hand, Sendai virus, PiggyBac Transposon, minicircle DNA, synthetic RNA and recombinant proteins are methodologically more complex and not so efficient, but much safer and therefore much more suitable for clinical purposes. Finally, plasmid-based alternatives are generally convenient and safe but with lower efficacy and therefore other alternatives are preferred.(Karagiannis et al., 2019)

1.3.1. Disease modelling with induced pluripotent stem cells

The development of iPSCs has made possible to obtain primary human tissue cultures never before obtained due to limited availability and accessibility of certain cell types (e.g. neurons) (Shi et al., 2017). iPSCs are scalable, with a great differentiating potential to model disease approximating real physiological conditions and thus providing more reliable data (Borger et al., 2017). They can be differentiated into various hard-to-obtain primary cell types in higher quantities and lastly, they can be generated from patient tissues, allowing us to retain the genetic and epigenetic hallmarks of the disease (Borger et al., 2017; Shi et al., 2017). Likewise embryonic stem cells can also serve this purpose but they are covered by very strict regulations, as well as heavy ethical implications. Therefore, making the use of iPSCs the preferred method (Shi et al., 2017).

Increasingly, there is a surge in the development of iPSC-derived models. The most popular cell type has been neurons, which is excellent since this is one of the cell types that was really lacking in the repertoire of cell models to study NPCD. Both because the disease is essentially neurological and neurons are heavily involved in its pathophysiology, and because existing mouse-derived neurons have a very different

physiology and biochemistry than that observed in humans (Ordoñez and Steele, 2017). For example, phenotypically, NPCD neurons of mice do not present accumulation of plaques or neurofrilliary tangles of tau and β-amyloid. Importantly, a neuronal iPSC-based model allows for the execution of high-thorughput drug screenings (Ordoñez & Steele, 2017; Völkner, Liedtke, Hermann, et al., 2021). Patient derived iPSC hepatocyte models have also been reported but on a much smaller scale, with the neurons, as of now being the power-house of patient derived iPSC models in NPCD (Maetzel et al., 2014; Völkner, Liedtke, Hermann, et al., 2021).

Patient derived-iPSC-based models generally showed concordance in intracellular cholesterol accumulation and corroborated previous findings in animal models, reinforcing its role as a disease hallmark and the validity and applicability of iPSC-based model systems NPCD disease modelling (Völkner, Liedtke, Hermann, et al., 2021). They also allowed to study and understand the impairment of autophagy in NPCD at a deeper level. For example, Maetzel et al (2014) found defective autophagic flux in iPSC-derived neurons and hepatocyte-like cells with an increase in autophagic vacuoles. Cell rescue was attempted via autophagy induction or cholesterol depletion that demonstrated an impact of cell type-specific drugs (Maetzel et al., 2014). Similarly, Dai et al (2017) found an impact on autophagic fusion autophagy flux in fibroblasts, neural stem cells and iPSC-derived neurons rescued by the use of methyl-β-cyclodextrin (Dai et al., 2017).

A study on glial cells derived from NPC1 patient derived-iPSCs has uncovered a little more about the phenomenon of gliosis, which is very common in neurodegenerative diseases, but still controversial in NPCD (Peter et al., 2017). Gliosis is the emergence of reactive astrocytes and microglia that normally act in a neuroprotective manner following cellular damage in the nervous system that upon chronic activation leads to cytotoxicity, culminating in neuronal death (Peter et al., 2017). Peter et al. (2017) found that their model system did indeed undergo gliosis, observing a significant increase in the amount of glial cells in the NPC1 mutant cell lines by an increase in GFAP (glial fibrillary acidic protein) positive cells and upregulation of vimentin and nestin. By blocking intracellular cholesterol transport with U18666A in control cells, gliosis was also triggered suggesting to be a result of the non-functional NPC1 protein. (Peter et al., 2017)

1.4. Macrophages

Macrophages are cells of the hematopoietic system, more specifically, innate immune cells that are found in all tissues and play a key role in inflammatory and homeostatic processes (Mosser and Edwards, 2008; Lyadova et al., 2021). Their main functions are to phagocytize pathogens, dead cells and debris. They are professional antigen-presenting cells to propagate an adaptive immune response as well as to secrete cytokines and proinflammatory mediators to further inflammatory response until its resolution (Gutbier et al., 2020; Lyadova et al., 2021). Afterwards, Macrophages are able to mediate tissue repair and heal by completely shift its phenotype and secrete anti-inflammatory and tissue remodelling cytokines (Lyadova et al., 2021).

These cells are highly plastic, undergoing a series of functional, morphological and biochemical changes dependent on its activation stimulus, which allows these cells to have a variety of tissue dependent functions (Mosser and Edwards, 2008; Wynn et al., 2013). Thus, when their functionality is affected, tissue repair and homeostasis become compromised being the cause or involved in several pathological processes such as, autoimmunity, chronic inflammation, cancer and degenerative diseases (Wynn et al., 2013).

Macrophages reside and perform their function primarily in their tissue of residence and when in need, circulating peripheral macrophages are recruited (Mosser and Edwards, 2008). These can be directly isolated from the tissue but it's not feasible. The use of animals is not the most adequate due to the great interspecies difference allied with the effect of tissue disaggregation and separation during the isolation that impossibilities the analysis of steady state "naive", also known as M0 macrophages (Lyadova et al., 2021). Immortalized cell lines are an option but lack biological significance with an oncological genetic background (Lyadova et al., 2021). Widely used and already discussed, human macrophages can be obtained by generation of monocyte derived macrophages.

For those reasons, the use of iPSC to generate macrophages seems a very attractive choice and, to date, to our knowledge, an iPSC derived macrophage disease model of NPC1 has not been published.

1.4.1. The different classes of macrophages and their biology

Most of tissue resident macrophages are created during embryonic hematopoiesis in the first two waves. The primitive hematopoiesis where primitive macrophages arise from the hemangioblast to form mainly microglia in the brain and the second wave, pre-definitive wave, in which the hemogenic endothelium is formed and erythromyeloid progenitors are generated that later originate macrophages that seed the leftover tissues and form self-renewing pools (Lee et al., 2018; Lyadova et al., 2021). The third wave, the definitive wave originates hematopoietic stem and progenitor cells that are the basis for adult hematopoiesis and consequently, peripheral macrophages (Lyadova et al., 2021).

When polarized by a stimulus, macrophages shift and acquire different characteristics, differing in receptor expression, cytokine and chemokine production as well as its functions (Funes et al., 2018; Mantovani et al., 2004).

Several attempts to categorize the different states of macrophages have been done, and up to now there is no consensus. One of the most commonly used classification, refers to its inflammation state, M1 and M2 macrophages with M2 constituting subsets. Initially macrophages were described as “classical” if stimulated by Interferon Gamma (IFN-γ)/Lipopolysaccharide (LPS) and “alternative” if stimulated by IL-4 (Murray et al., 2014). Later M1 and M2 terminology was introduced correlating its activation state with Th (T helper) 1 and 2 responses (Martinez and Gordon, 2014). However, these approaches seem very reductive for the abundance of macrophages with different phenotypes. To the later terminology it was suggested to expand the M1 and M2 terminology to account for different activation scenarios, adding M2 subsets (M2a, M2b, M2c, M2d) (Murray et al., 2014).

M1 macrophages exhibit a pro-inflammatory phenotype by producing toxic intermediates, reactive oxygen intermediates (ROI), nitric oxide (NO), and chemokines and cytokines that recruit immune cells to propagate and generate an adaptive response, such as IL-1, IL-6, IL-12, CXCL9, CXCL10 (K. Y. Lee, 2019). In that sense, M1 display a critical role in fighting back acute infections mediated by pathogens or tumours and it is induced by cytokines such as IFN-γ or PAMPs (pathogen-associated molecular patterns) like LPS (lipopolysaccharide) or endogenous danger signals (Funes et al., 2018).

M2 macrophages also known as alternative activated macrophages, have shown to be an increasingly diverse group. Macrophages can be induced by several types of stimuli and generate a variety of macrophages with different functions and transcriptional profiles. Hence, M2 macrophages, remain a challenge to categorize. Mantovani et al (2004) proposed to use the generic term of M2 for the remaining forms of macrophage activation besides M1, categorizing them as M2a, M2b, M2c.

M2a macrophages are stimulated by IL-4 and IL-13, are characterized by a predominance of the arginase pathway and production of chemokines largely associated with a more anti-inflammatory response such as CCL24, CCL22, CCL17 and CCL18, as well as inhibition of pro-inflammatory chemokines associated with IFN-γ activation (Mantovani et al., 2004). In general, M2 stimuli inhibit the pathways or divert them from producing M1 associated chemokines and cytokines and vice-versa. These macrophages seem to promote a Th2 and type II inflammation response, involved in allergy, killing and encapsulation of parasites(Funes et al., 2018; Mantovani et al., 2004).

M2c macrophages are stimulated by IL-10 and TGF-β (transforming growth factor-beta) and similarly to M2a, are characterized by a predominance of the arginase pathway with a production of CCL18, CCL16 and CXCL13 suggested to have a role in promoting matrix deposition, tissue remodeling and immunoregulation (K. Y. Lee, 2019; Mantovani et al., 2004). M2b macrophages are stimulated by Immune complexes (IC)

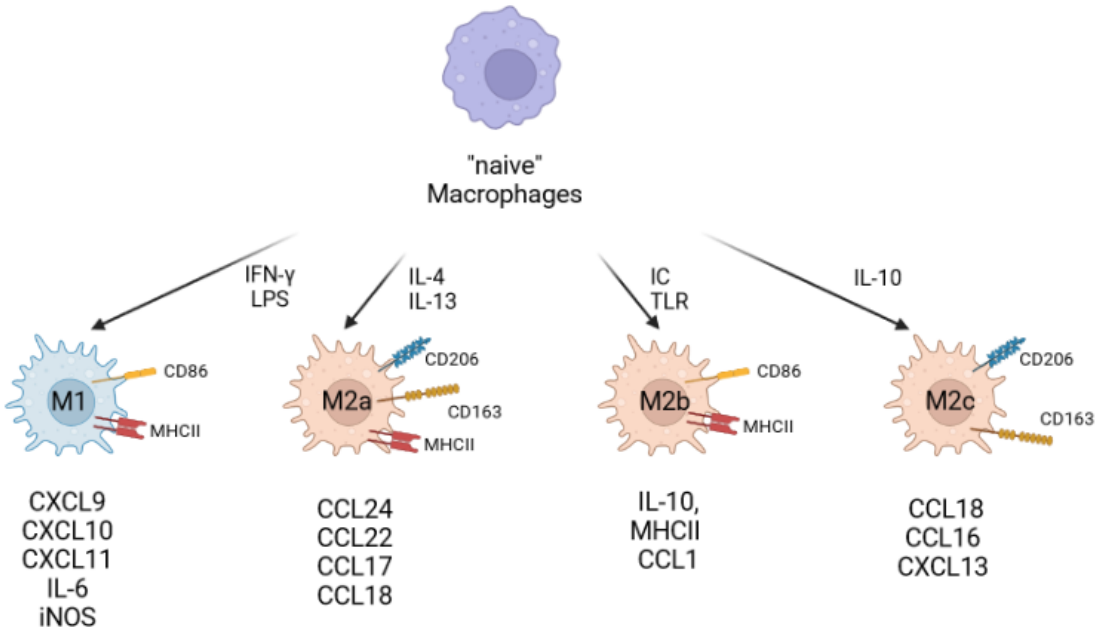

Figure 5- Overview of the most described polarization status of macrophages with respective stimulus and representative surface markers and produced cytokines/chemokines for each subset. Created in BioRender.com.

and toll-like receptor (TLR) agonists (Funes et al., 2018). Unlike the two previous categories, retain some level of a pro-inflammatory phenotype. They do not possess the arginase pathway upregulated, and express high levels of IL-10, MHCII (major histocompatibility complex class II) and CD86 and low levels of IL-12(Mantovani et al., 2004). Despite that, they lead to Th2 activation and antibody production due to an increased production of CCL1 (Mantovani et al., 2004).

More evidence regarding other types of polarization that are not categorized in these groups is emerging such as macrophages induced by adenosine A_{2A} and TLR receptor agonists, promoting angiogenesis and apoptotic clearance, M4 macrophages induced by CCL4, Mhem macrophages induced by haemoglobin, and more (Funes et al., 2018).

In this work, only IL-4 induced macrophages will be discussed, therefore for simplification purposes, these will be referred simply as M2 macrophages.

These phenotypes are modulated by key pathways. JAK/STAT is implicated in many cytokine mediated responses including the crucial IFN-γ, indicating a fundamental role in M1 modulation, as well IL-4 signaling, exacerbating its importance. Further, NFkB is a key transcription factor for induction of inflammatory genes such as, IL-1b, IL-6 and TNF-α in M1 macrophages (T. Liu et al., 2017). Additionally, PI3k/Akt regulates several cellular mechanisms such as viability, motility, proliferation and metabolism, seeming to be essential to support macrophage survival (Zhou et al., 2014). Different effector Akts result in different polarization phenotypes, AKT1 being essential to shift macrophage into an inert phenotype and ablation of AKT2 leads to an M2 phenotype (Zhou et al., 2014) . These are some of the important few.

1.4.2. Macrophages in Niemann-Pick disease Type C

NPCD is associated with the presence of foamy cells in the bone marrow and NPC1 is essential for proper function of macrophages. It is acceptable to believe that these immune defects further exacerbate inflammatory responses that contribute to the progression of the disease (Lopez et al., 2012).

To date, a few articles have studied macrophages in an NPCD context. (Lopez et al., 2012). They report abundant foamy macrophages in alveolar spaces (Muralidhar

et al., 2011), heavilly affected cholesterol trafficking (Reid et al., 2003) and appear to be heavily implicated in visceral pathology (Rimkunas et al., 2009).

More recently, a study in microglia, tissue resident macrophages of the brain, has attempted to elucidate the role of this cell type in NPCD and how the disease affects it (Colombo et al., 2021). Restoring NPC1 expression in neurons alone does not reverse the disease phenotype, indicating that NPCD affects other neuronal cell types. NPC1 is highly expressed in microglia, the resident immune cells of the central nervous system whose have a key role during brain development (Colombo et al., 2021). The study showed that loss of NPC1 induced microglia into a state of "disease-associated microglia," severely impairing their function alongside with defects in lipid trafficking and cholesterol accumulation (Colombo et al., 2021).

Unfortunately, mouse microglia were used and to compensate the study explored monocyte-derived macrophages acquired via blood samples. These have been shown to recapitulate the findings in murine microglia, such as similar changes in proteomic signatures as well as trafficking defects that may result in key phenotypic features of myelin degradation, indicating that macrophages may represent a valuable model for studying NPCD (Colombo et al., 2021).

However, this study used macrophages derived from monocytes acquired from blood samples. Typically, this method isolates CD14+ monocytes that are then differentiated into macrophages by the addition of small molecules (SM). Although it is a easily accessible model, the cells are non-proliferative and cannot be maintained for long-term culture, which makes it scarce. Therefore, not only is it not scalable as well as it does not accurately represent the physiology of resident macrophages. (Lyadova et al., 2021)

Hence, being one of the affected cell types showing a distinct phenotype and given its central role in immune responses, an iPSC-derived macrophage model for NPCD can be of great relevance.

1.4.3. Induced pluripotent stem cell derived macrophages

In a way, macrophage generation from iPSCs resembles embryonic haematopoiesis. There are 3 main types of procedures to generate iMph (iPSC-derived macrophages), EB-based (3D), which can be spontaneous or factor assisted and EB-

independent 2D factor assisted protocols (Lyadova et al., 2021). Overall, the different procedures culminate in a similar sequence of events. A mesoderm commitment and hemogenic endothelium differentiation is induced by the use of basic morphogenic protein 4 (BMP4) for induction of mesoderm, vascular endothelial growth factor A (VEGF) which is related to hemangioblast formation as well as expansion and differentiation of hematopoietic progenitors and lastly, stem cell factor (SCF) necessary for progenitor proliferation (Lyadova et al., 2021). M-CSF and IL-3 that induces endothelial-to-hematopoietic transition, generation of hematopoietic progenitors and myeloid specification simultaneously generating macrophage precursors that then are suffer a final differentiation into macrophages (C. Z. W. Lee et al., 2018; Lyadova et al., 2021).

Initial transcriptomic analysis indicated a relation with blood-derived monocytes, meaning that these methods would originate monocyte-derived macrophages and therefore unable to model tissue resident macrophages (C. Z. W. Lee et al., 2018).

More recently, new studies came to suggest otherwise. Buchrieser et al (2017) showed that iPSC-derived macrophages develop in similarity with the first wave of embryonic haematopoiesis, the primitive wave by evolving in an MYB-independent and RUNX1-dependent fashion. This indicates that iMph can be suitable for modelling tissue/resident macrophages such as microglia, Kupffer cells and others (Buchrieser et al., 2017; C. Z. W. Lee et al., 2018).

To date, we are not aware of any studies using patient-derived iPSC macrophages for NPC1. With this information in mind and the fact that foam cells constitute one of the phenotypic features in patients with NPCD, this work attempts to fill this gap by generating and characterizing a model system of patient-derived iPSC macrophages.

Chapter 2

Aims

2. Aims

With the aim to accurately diagnose, understand and treat rare genetic, metabolic and neurodegenerative diseases, Centogene settled on a mission to “enable the cure of 100 rare diseases in 10 years” (About Us: The CENTOGENE Story) being NPCD one of the focused diseases. As NPCD therapies are scarce and lack efficiency, patients are not able to significantly expand their life expectancy leading to an early dead, urging for better alternatives to improve these patients lives.

Therefore, this internship falls under the R&D project on NPCD, regarding cellular models and drug development with the aim of evaluating, characterizing the disease model and generating data to contribute to the Bio/Databank to further our knowledge in the disease and attempt to develop or discover a compound that can be used in a cure or treatment more effective than the current market alternatives.

Thus, the main goal of this work passes through:

1. Protocol characterization and assessment of iMph identity.
2. Assessment of iMph functionality including polarization potential.
3. Assessment of key NPCD phenotypical features and ability to model the disease.

Chapter 3
Materials and Methods

3. Materials and Methods

3.1. Characteristics of induced pluripotent stem cell lines

Centogene receives thousands of biological samples to diagnose from all over the world, which are used to broad its own Bio and Databank. This allows Centogene to generate knowledge and better understand the diseases so they can constantly improve their diagnostic capabilities and offer insight for drug discovery.

From this Biobank, both patient fibroblast lines with the mutation of interest and control lines (disease carriers) were selected. Cells were reprogrammed in house into iPSCs with CytoTuneTM 2.0 Sendai Reprogramming Kit (Invitrogen™), maintained in Matrigel® (Corning®) coated plates, cultured with mTESR™ Plus (STEMCELL™ Technologies) medium and passaged with 10mM EDTA.

iPSC lines were characterized in-house by various methods, importantly, for Tra-1-60, SSEA-4, OCT3/4, SOX2, SSEA-1 through flow cytometry and for trilineage germ layer genes such as CXCR4, GATA6, CDH1, HES5, PAX6, DCX, GATA2, BMP-4 and IGF2 by qPCR (Real time polymerase chain reaction). Genotyping was done by whole genome sequencing and genetic identity was assessed by STR (Short Tandem Repeat profile).

Table 1- Genotypic characteristics and clinical information of the iPSC lines used throughout this work.

Line Id	Type	cDNA position	Amino acid position	Clinical information
C01	Carrier	c.1610T>C	p.Phe537Ser	-
C02	Carrier	c.3503G>A	p.Cys1168Tyr	-
P01	NPC1	c.1628delC	p.Pro543Argfs*20	• Neurological symptoms • Intellectual disability • Splenomegaly • Hepatomegaly • Elevated hepatic transaminases • Abdominal distention • Prolonged neonatal jaundice • Mild global developmental delay
P02	NPC1	c.3503G>A	p.Cys1168Tyr	• Splenomegaly • Hepatomegaly • Neurological symptoms • Neonatal icterus

- Failure to thrive in the toddler period

iPSC patient 01 line has a deletion of a cytosine residue in position 1628, leading to a frameshift type of mutation with a premature stop codon (PTC) and a change from proline to arginine in position 543 of the protein.

iPSC patent 02 line has a missense substitution in residue 3503 of a guanine to adenosine, leading to a tyrosine instead of a cysteine in position 1168 of the protein.

3.2. Induced pluripotent stem cells culturing and expansion

mTeSR Plus (StemCell Technologies) and Matrigel® (Corning Life Sciences) were prepared according to manufacturer guidelines.

iPSCs lines were cryopreserved in CryoStor10 (StemCell Technologies). They were quickly thawed and diluted with three times the volume of DMEM/F12 (Gibco), resuspended in mTeSR Plus (StemCell Technologies) and plated in Matrigel® (Corning Life Sciences) coated 6 well-plates. Incubation at 37ºC and 5% CO_2.

Medium was changed every other day and cells were checked every day until 70%-80% confluency was achieved for passage.

Cells were chemically passaged using 0.5mM ethylenediaminetetraacetic acid EDTA at a concentration of 0.5mM EDTA. Following dissociation into smaller colonies, cells were plated on Matrigel® (Corning Life Sciences) coated plates in a cell line dependent proportion based on each iPSC line's proliferation rate.

3.3. Macrophage generation and maintenance

Aiming for culture synchrony, iPSCs were thawed and passaged as previously described until a confluency of 70%-80% was achieved

- **EB Formation**

An EB-based 3D factor-assisted protocol was used. To that end, iPSCs colonies were broken into single cells with Accutase (SIGMA) and counted in a Neubauer chamber using trypan-blue (Life Technologies). Cells were resuspended in mTeSR Plus

(StemCell Technologies) medium supplemented with 10μM Y-27632, 50 ng/ml basic morphogenic protein 4 (BMP4), 50 ng/ml vascular endothelial growth factor A (VEGF) and 20 μg/ml stem cell factor (SCF) in order to direct differentiation into mesoderm commitment. EB generation was carried out in a 96 well round bottom plate coated with Anti-Adherence Rinsing Solution (STEMCELL Technologies). EB's morphology was checked under the microscope and incubated at 37°C with 5% CO_2.

On the two following days a 50% medium change was performed with EB medium (mTeSR Plus (StemCell Technologies) supplemented with BMP4, VEGF and SCF in the same concentration as previously used) and EBs were left undisturbed until day 4 post seeding.

- **EB Replatting**

EBs were replated into 0.1% gelatin (Sigma-Aldrich) coated cell culture flasks with X-Vivo15 (LONZA) medium supplemented with 1% of 5,000 U/mL Penicillin/Streptomycin (Gibco™), 1% of 200mM L-Glutamine (Thermo Fisher) and 0,1mM β Mercapto-ethanol (Thermo Fisher). 50 ng/ml of human M-CSF (Miltenyi) and 25 ng/ml of human IL-3 (Miltenyi) were freshly added to the supplemented medium. Medium was changed on day 4 and left undisturbed until day 8 post seeding.

- **Medium change and collection of precursors**

Every 3 to 4 days a 75% medium change was performed with supplemented X-Vivo15 (LONZA) and freshly added SM as previously described.

Around the 2nd week mark, EBs started producing macrophage precursors. Henceforth, precursors were collected in low attachment cell culture flasks coated with 2% (w/vol) Poly(2-hydroxyethyl methacrylate) (Sigma-Aldrich) and maintained in culture circa 3 months, during which time cells underwent quality control which will be addressed further below.

- **Macrophage Maturation**

To obtain mature macrophages, precursors suffered a 7day maturation by exposure to high concentrations of M-CSF (100ng/ml). Precursors were seeded in the desired confluency, depending on the objective of the experiment and the type of plate used, with RPMI 1640 w/ GLUTAMAX I (Gibco™), supplemented with 1% of 200mM L-Glutamine (Thermo Fisher), 1% of 5,000 U/mL Penicillin/Streptomycin (Gibco™), and

10% Fetal Bovine Serum (FBS, Sigma-Aldrich). Incubation was taken ahead at 37°C with 5% CO_2 and medium was changed on day 3 or 4.

3.4. Immunocytochemistry

Macrophages were firstly fixed with 4% Paraformaldehyde (PFA) in Dulbecco's phosphate-buffered saline (DPBS) (Thermo Fisher) at RT for 20 minutes. After permeabilization with 0,25% of Triton-X 100 (Sigma-Aldrich) in DPBS (Sigma-Aldrich) for 10 minutes, cells were washed once and incubated for an hour in Blocking Solution - 3% Bovine Serum Albumin (Miltenyi Biotec) or 5% Donkey Serum (Chemicon®) in DPBS (Sigma-Aldrich) according to secundary's host species. Primary antibodies were added in blocking solution and incubated overnight at 4ºC in constant subtle agitation. Cells were washed and incubated with the secondary antibody in blocking solution for an hour at room temperature. A list of the used antibodies in the respective concentration can be found in table 2. After washing and, in preparation for image acquisition, desired nuclear/cytoplasmic stains were added according to manufacturer's instructions, and finalized with addition of DPBS. For Anti- Niemann Pick C1 antibody specifically, permeabilization was carried out in 0.2% Tween®20 (Carl Roth®) in DPBS and incubated at RT for an hour. The remaining steps were performed as described.

A table regarding the different stains used throughout this work can be found in table 3. Images were acquired in ImageXpress Micro Confocal High-Content Imaging System (Molecular Devices) and quantification was taken ahead in MetaExpress Software.

A custom quantification module was designed, individual cells were segmented using the cell mask and nuclear marker Hoechst. First a fluorescence threshold was set to highlight the nucleus, then the dimensions and intensity above the local background were set for the nucleus as well as for the cell outline. These images were combined to build two binary masks that segment the cells and show the contour of each individual cell. Border objects were removed, and the average NPC1 and LAMP2 protein signal intensity was measured.

Data was exported in excel files and statistically analysed using GraphPad Prism Software v8.3.0.

Table 2- List of primary and secondary antibodies used throughout this work.

Antibody	Concentration	Host Species	Catalog #	Company
Recombinant Anti-Niemann Pick C1 antibody [EPR5209]	1:70	Rabbit	ab134113	Abcam
H4B4, LAMP-2 (human, supernatant)	1:60	Mouse	-	DSHB
Recombinant Anti-LAMP1 antibody [EPR24395-31]	1:500	Rabbit	ab278043	Abcam
Anti-Perilipin 2 (N-terminus aa 1-29) guinea pig polyclonal, serum	1:200	Guinea Pig	GP40	PROGEN Biotechnik GmbH
Goat anti-Guinea Pig IgG (H+L) Highly Cross-Adsorbed Secondary Antibody, Alexa Fluor™ 488	1:1000	Goat	A11073	Invitrogen™
Goat anti-Mouse IgG (H+L) Cross-Adsorbed Secondary Antibody, Alexa Fluor™ 568	1:1000	Goat	A11004	Invitrogen™
Donkey anti-Mouse IgG (H+L) Highly Cross-Adsorbed Secondary Antibody, Alexa Fluor™ 647	1:1000	Donkey	A31571	Invitrogen™
Donkey anti-Rabbit IgG (H+L) Highly Cross-Adsorbed Secondary Antibody, Alexa Fluor™ 568	1:1000	Donkey	A10042	Invitrogen™
Donkey anti-Rabbit IgG (H+L) Highly Cross-Adsorbed Secondary Antibody, Alexa Fluor™ 488	1:1000	Donkey	A21206	Invitrogen™

Table 3- List of stains used throughout this work.

Stain	Concentration	Incubation period	Filter Set	Catalog #	Company
HCS CellMask™ Red Stain	2µg/ml	30'	Texas Red	H32712	Invitrogen™
HCS CellMask™ Green Stain	2µg/ml	30'	FITC	H32714	Invitrogen™
eBioscience™ DRAQ5™	2µM	30'	CY5	65-0880-92	Invitrogen™
Hoechst 33342 Solution (20 mM)	4µM	15'	DAPI	62249	Thermo Scientific™

3.5. Quality control for induced pluripotent stem cell derived macrophages

3.5.1. Flow Cytometry for expression of surface markers

To evaluate macrophage's identity, a quality control of the surface markers was performed around 4 weeks and 20 weeks post beginning of production. CD14, CD45, CD68, CD86 and CD163 markers were used, information regarding the used antibodies can be found in table 4. Matured cells were harvested using 10mM EDTA and resuspended in staining buffer - MACSQuant Running Buffer (PBS, EDTA, Stabilizer, 0.09% Sodium Azide) with 0,5% BSA, 2mM EDTA. Sample was then divided into 4 tubes and the following antibody mixes were added: unstained (no antibodies), CD14-CD68, CD45-CD163, CD86. Incubation was carried out for 10 minutes at 4ºC protected from light. The compensation settings were acquired using the MACS® Comp Bead Kit, anti-REA (Miltenyi Biotec) and the unstained sample as control. Samples were acquired in the MACSQuant® Analyzer 10 (Miltenyi Biotec) and all data was analyzed in Flowjo v10.6.0.

Table 4- List of conjugated antibodies used throughout this work for flow cytometry.

Antibody	Concentration	Conjugate	Catalog #	Company
CD14 Antibody, anti-human, REAfinity™	1:50	FITC	130-110-576	Miltenyi Biotec
CD45 Antibody, anti-human, REAfinity™	1:50	PE	130-110-770	Miltenyi Biotec
CD68 Antibody, anti-human, REAfinity™	1:50	APC	130-114-652	Miltenyi Biotec
CD86 Antibody, anti-human, REAfinity™	1:50	FITC	130-116-262	Miltenyi Biotec
CD163 Antibody, anti-human, REAfinity™	1:50	VioBlue	130-112-134	Miltenyi Biotec

3.5.2. Functional Assay

Mature macrophages were incubated for an hour with TransFluoSpheres™ Carboxylate-Modified Microspheres, 1.0 µm (488/560), 2% solids (Invitrogen™) in a proportion of 2.5ul per ml of medium. Both control cells (no incubation with spheres) and cells with spheres were harvested using 10mM EDTA, washed with PBS and resuspended in staining buffer (MACSQuant Running Buffer (PBS, EDTA, Stabilizer, 0.09% Sodium Azide), 0,5% BSA, 2mM EDTA). Samples were acquired in the MACSQuant® Analyzer 10 (Miltenyi Biotec) and all data was analyzed in Flowjo v10.6.0.

3.5.3. Evaluation of Cholesterol levels

Mature macrophages were fixed, and PFA residues were neutralized with 1.5 mg/ml glycine in DPBS for 10 minutes at RT. Following that, Filipin III ready-made solution 1mg/ml (Sigma-Aldrich) was added in a concentration of 0.05 mg/ml, incubated for 55 minutes and washed. Desired extra dyes (table 3) were added as a last step. Images were acquired in ImageXpress Micro Confocal High-Content Imaging System (Molecular Devices), right away as filipin staining easily photo-bleaches. Nile red staining was done using Nile Red Staining Kit (Abcam #ab228553) following the manufacturer's guidelines for fixed cells. Quantification was taken ahead in MetaExpress Software (Molecular Devices).

A custom quantification module was designed, individual cells were segmented using cell mask and a nuclear marker. First, a fluorescence threshold was applied to highlight the nucleus, then the dimensions and intensity above the local background were set for the nucleus as well as for the cell outline. These images are combined to construct two binary masks that segment the cells and show the contour of each individual cell. Artifacts were removed by applying an intensity threshold. Filipin vesicles were highlighted based on pixel shape and size, then the width and intensity dimensions above the local background were set to create a Filipin mask. The boundary objects were removed, the filipin mask was applied to the segmentation mask. The average filipin intensity per cell and the average filipin vesicle area per cell were measured.

Data was exported in excel files and statistically analysed using GraphPad Prism Software v8.3.0.

3.6. Sample preparation for transcriptomics

Cells were seeded in triplicates and in high density to make sure there was enough sample for the RNA extraction and subsequent use for RNA sequencing, polarized for 7 seven days with a medium change at the 3rd day post seeding (-d04). RPMI medium supplemented with 10% FBS, 1% Pen/Strap, 1% L-Glutamine and specific SM was used. SM's type and concentration for each type of polarization were chosen as described by Gutbier et al (2020) and can be found in table 5.

Table 5- Experimental details regarding small molecules used for each condition and respective concentration to induce macrophage polarization.

Polarization status	Small Molecules (SM)	Concentration of Small Molecules
M0	M-CSF	100 ng/ml
M1	GM-CSF	100 ng/ml
	IFN-γ	50 ng/ml
M2	M-CSF	100 ng/ml
	IL-4	50 ng/ml

At day 0 cells were harvested in RNA Lysis Buffer (component of Quick-RNA™ Microprep Kit, Zymo Research) and kept at minus -80C until further processing.

- **RNA extraction and sequencing**

RNA extraction and sequencing was taken ahead by the Genomic Research and Development Department. Total RNA extraction was performed with Quick-RNA™ Microprep Kit (Zymo Research) following the manufacturer's instructions. RNA was quantified with Qubit RNA High Sensitivity kit (Qubit Fluorimeter WI-27, Invitrogen™) and its quality assessed using Agilent RNA Screentape (TapeStation, Agilent). RNA integrity ranged from 9.8 to 8.4, indicating a good quality RNA overall.

Library preparation for sequencing was done using Illumina Stranded mRNA Prep, Ligation (Illumina®) with IDT-ILMN Nextera DNA UD Indexes (96 Indexes) Set A. Before sequencing, the library suffered a quality control by means of Agilent DNA 1000 (Agilent Technologies). After pooling, the library was sequenced with Illumina NextSeq500/550 High Output kit on NovaSeq 6000 system for 150 cycles.

- **Computational Analysis**

Treatment of the raw data was taken ahead by the Bioinformatics department. Raw data were obtained directly from the sequencer and converted to FASTQ-files with bcl2fastq(bcl2fastq Conversion Software) software v2.20.

Reads were mapped to the human reference genome GRCh37 (release date: 27/02/2009) by using Spliced Transcripts Alignment to a Reference (STAR) (GitHub - alexdobin/STAR: RNA-seq aligner; Dobin et al., 2013)v2.7.10a. The quality of the reads was checked by Picard(Picard Tools - By Broad Institute) v2.27.4 and FastQC (Babraham Bioinformatics - FastQC A Quality Control tool for High Throughput Sequence Data, no date) v.0.11.9. Samples with >30M of total reads and >20M of mapped reads were taken into consideration.

The aligned reads were counted using feature counts (Liao et al., 2014) v.2.0.2, and genes with low counts (<20) were filtered out. The gene count data were normalized and analysed using DESeq2 v. 1.36.0 (Love et al., 2014). Each gene was modelled by employing a negative binomial linear model, and a Wald test was applied to test for significance(Love et al., 2014).

In DESeq2, it was assessed the differences between polarization states in control samples, as well as differences between control and disease samples in a certain polarization state. The differential expression was given in log2 fold change (FC), and the adjusted p-value was calculated based on the False Discovery Rate (FDR) method by Benjamini and Hochberg (Benjamini and Hochberg, 1995). To consider differentially expressed genes (DEG), a threshold for the absolute log2 FC was set at above 0.58 and below -0.58 and an adjusted p-value lower than 0.05.

Functional analysis was done through Ingenuity Pathway Analysis (IPA) cloudware (QIAGEN, www.qiagen.com/ingenuity), to identify pathways and functional networks among DEG. The DEG were also analysed on KEGG Pathway Database (Kanehisa Laboratories, https://www.genome.jp/kegg/) for the main involved pathways in NPC1 disease, such as sphingolipid metabolism, lysosomes, autophagy and inflammatory pathways.

The datasets generated and analyzed are the intellectual property of Centogene GmBH.

3.7. Statistical Analysis

Statistical analysis was carried out in GraphPad Prism v8.3.0 (GraphPad Software, San Diego CA). Data is expressed as mean ± SEM (Standard Error of Means) or mean ± SE(Standard Error) if mentioned in the text. Differences between groups were examined by Kruskal-Wallis-Test with Benjamini-Hochberg for multiple hypothesis correction, p-value<0.05 was considered to be statistically significant.

Chapter 4

Results and Discussion

4. Results and Discussion

4.1. Induced pluripotent stem cells expansion and macrophage generation

First step of generation of human iMph goes through the formation of embryoid bodies (EB) from iPSCs, they are three-dimensional (3D) cell aggregates that form the three germ layers of the embryo and mimic its spatial organization (Lim et al., 2013) A spin-EB technique was used, in which cells were centrifuged in round bottom low attachment plates. This technique increases the efficiency of EB formation and yields well defined and round EBs (van Wilgenburg et al., 2013; Hale et al., 2015). A general overview of the protocol and its different stages can be found in figure 6.

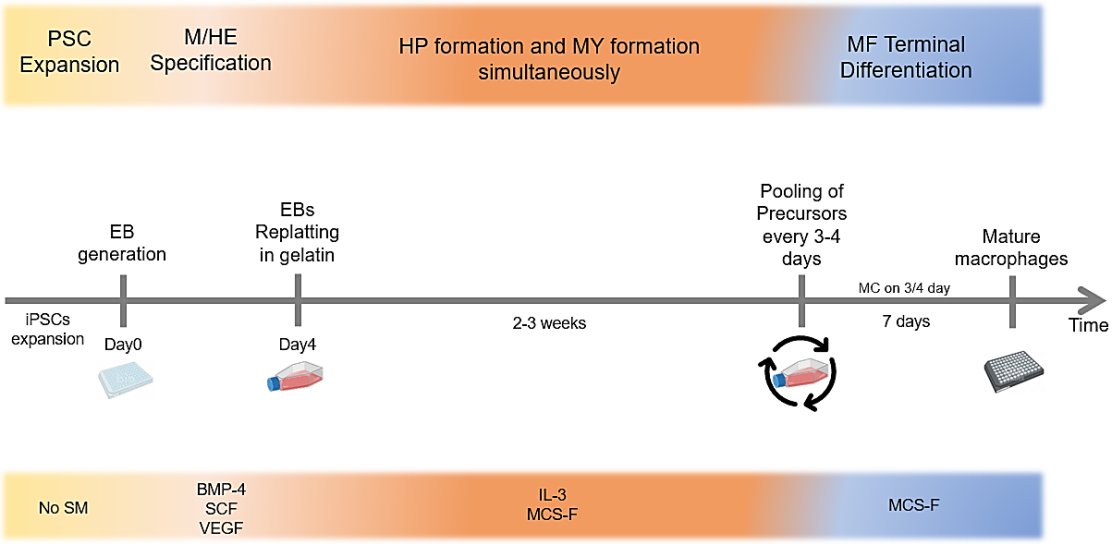

Figure 6- Schematic view and timeline of the generation of macrophages from iPSC stage to mature macrophages. On the top, the corresponding different four main stages of differentiation can be observed as well as in the bottom, the SM inducers of that same differentiation stage. PSC-Pluripotent stem cell; M/HE-Mesoderm commitment and Hemogenic Endothelium; HP-Hematopoietic Progenitors; MY-Myeloid Specification; MF-Macrophage Final differentiation.

As observed in figure 7, iPSCs presented their characteristic morphology, showing highly compact cells with a well-defined border and no apparent signs of differentiation (Rivera et al., 2020). EBs presented a round shape post-seeding, similar in size with some differences between different iPSC lines (figure 7, day 0), likely due to small counting inaccuracies. For four days EBs had medium change with BMP4, SCF and VEGF to induce mesoderm commitment and hemogenic endothelium differentiation.

By the end of this period, the protocol showed to be highly robust with all EBs presenting a compact and homogeneous morphology (figure 7, day 4), and a yield of 100% (no EBs were lost or discarded). This is in line with what was expected, not only presenting comparable morphology to what is described by van Wilgenburg et al (2013) protocol but also allied with the improved yield reported by Gutbier et al. (2020).

After four days, some cells were already visible in the supernatant of the EB flasks and, 2-3 weeks after replating, those were harvested henceforth until EBs were discarded. This endpoint was determined based on production yield and overall cell state which decreases significantly at around the 2 months and half mark in accordance with other protocols (Gutbier et al., 2020; Lopez-Yrigoyen et al., 2020).

Macrophage precursors suffered a final differentiation step into macrophages using high M-CSF concentration. Such conditions induce the transition from a rounder shape to an elongated morphology with the exhibition of multiple processes (Figure 7, mature macrophages). Importantly, other published protocols, in which this final differentiation stimulus is present, report similar morphological features, characteristic of fully functional macrophages (McWhorter et al., 2013; Rostam et al., 2017).

Regarding total yield, it varied through different iPSC material, from 116x to 200x per input of iPSC material. Initially we hypothesised that the use of patient derived iPSC would result in a lower yield than the carrier counterpart, however such correlation was not observed. In our experience, the outcome seemed to be dependent on the quality of the starting material (ex. presence of differentiation), as well as their confluency, which aligns with other authors' findings (Lopez-Yrigoyen et al., 2020).

The use of X-Vivo15 medium during the generation of the iMph allows for a serum-free condition which highly reduces variability during model generation. However, the last differentiation step of the presented protocol still occurs under serum supplemented conditions as its use is well documented. To decrease variability further, an X-Vivo15 differentiation could be tested and explored as it seems to offer good results and it is an important factor to consider when performing high-throughput (HT) drug screenings. Moreover, it has been already tested by some authors with success (van Wilgenburg et al., 2013; Gutbier et al., 2020).

Overall, this EB-based factor assisted protocol allows for easy and prolonged cultivation in serum-free conditions with a high yield. Furthermore, its robustness makes it potentially scalable for HT experiments that serve as basis for drug discovery.

Buchrieser et al (2017) showed that macrophages generated by this kind of protocol seem to derive from Myb-independent yolk sak progenitors, the same origin as tissue resident macrophage like microglia and Kupffer cells.(Buchrieser et al., 2017) In this case, mesoderm commitment and hemogenic endothelium specification happen simultaneously. Some protocols follow this EB-based factor assisted approach but have sequential mesoderm commitment and hematopoietic specification (Lyadova et al., 2021). EBs are formed in suspension and its mesoderm induction is driven by BMP-4, VEGF, SCF, TPO (Thrombopoietin), FIt3 (Fms-related tyrosine kinase 3 ligand) and bFGF (basic fibroblast growth factor), followed by hematopoietic specification driven by VEGF, SCF, TPO, Flt3 and bFGF and both myeloid expansion and macrophage differentiation are done in serum dependent condition with M-CSF (Lim et al., 2013; Martinez et al., 2006). This results in a laborious and more complex protocol with higher cost, as well as a one-off harvest of macrophages and low yield (~6x the iPSC input) (Lyadova et al., 2021).

EB-based spontaneous protocols have mesoderm commitment and hematopoietic endothelium specification along with EB formation, cell clusters of iPSCs are pooled together and incubated in low adhesion conditions under orbital rotation to favour cell aggregation (Ackermann et al., 2018). This leads to limited reproducibility as it depends on parameters that are not well defined and are difficult to control such as EB size (Lyadova et al., 2021). Furthermore, stem cells for this approach are maintained in feeder dependent conditions which decreases its suitability for clinical settings (Lyadova et al., 2021).

Lastly, two-dimensional (2D) factor assisted protocols have a more diverse methodologic approach regarding the factors used to drive haematopoiesis. These are quite similar to EB-based factor assisted approach with sequential mesoderm commitment and hematopoietic specification but rather added directly to colonies of iPSC which later results in floating cells that are pooled together and transferred to low attachment plates for myeloid specification (Cao et al., 2019; Lyadova et al., 2021). Cao et al (2019) protocol has the advantage of generating monocyte-like cells in only 15 days and was also able to cryopreserve these cells with a recovery rate of circa 40%, which ultimately results in a low yield allied to the one-off harvest. This leads to one of the main challenges of most of these macrophage generation approaches – cryopreservation efforts of both progenitor and matured macrophages present low recovery rates and viability (Gutbier et al., 2020; Lopez-Yrigoyen et al., 2020). Ideally, one big batch of iMph

would be produced and cryopreserved to keep consistency through experiments. This way we minimize batch effect which can heavily affect cells characteristics in a substantial manner, leading to irreproducible results. In an attempt to address this issue, Munn et al (2021) recently developed a protocol in which cells were cryopreserved both as hematopoietic progenitors and matured cells, having achieved a high recovery rate (around 75% from inference of supplementary figures) and high viability (almost 100%). In this case, hematopoietic differentiation was started by forming iPSC cell aggregates for 24h followed by supplementation with FGF, BMP4 and VEGF for 5 days to induce mesoderm commitment, followed by supplementation with Fit-3, TPO, SCF, IL-3, IL-6 for 8 days originating hematopoietic progenitors' cells (HPC) which were dissociated and purified with CD34 beads and cryopreserved in CryoStor10 using a Control Rate freezer (Munn et al., 2021). For further differentiation, HPCs were expanded into common myeloid progenitors and further differentiated into macrophages with M-CSF and IL-1β. These matured macrophages were cryopreserved as well in the same manner(Munn et al., 2021). However, this is a more expensive and laborious protocol, which might not be suitable for high-throughput purposes in a company setting.

At the moment, the alternative solution is based on the ability to keep precursor cells in culture for a long period of time with high yields in each harvest, two important aspects covered by our protocol.

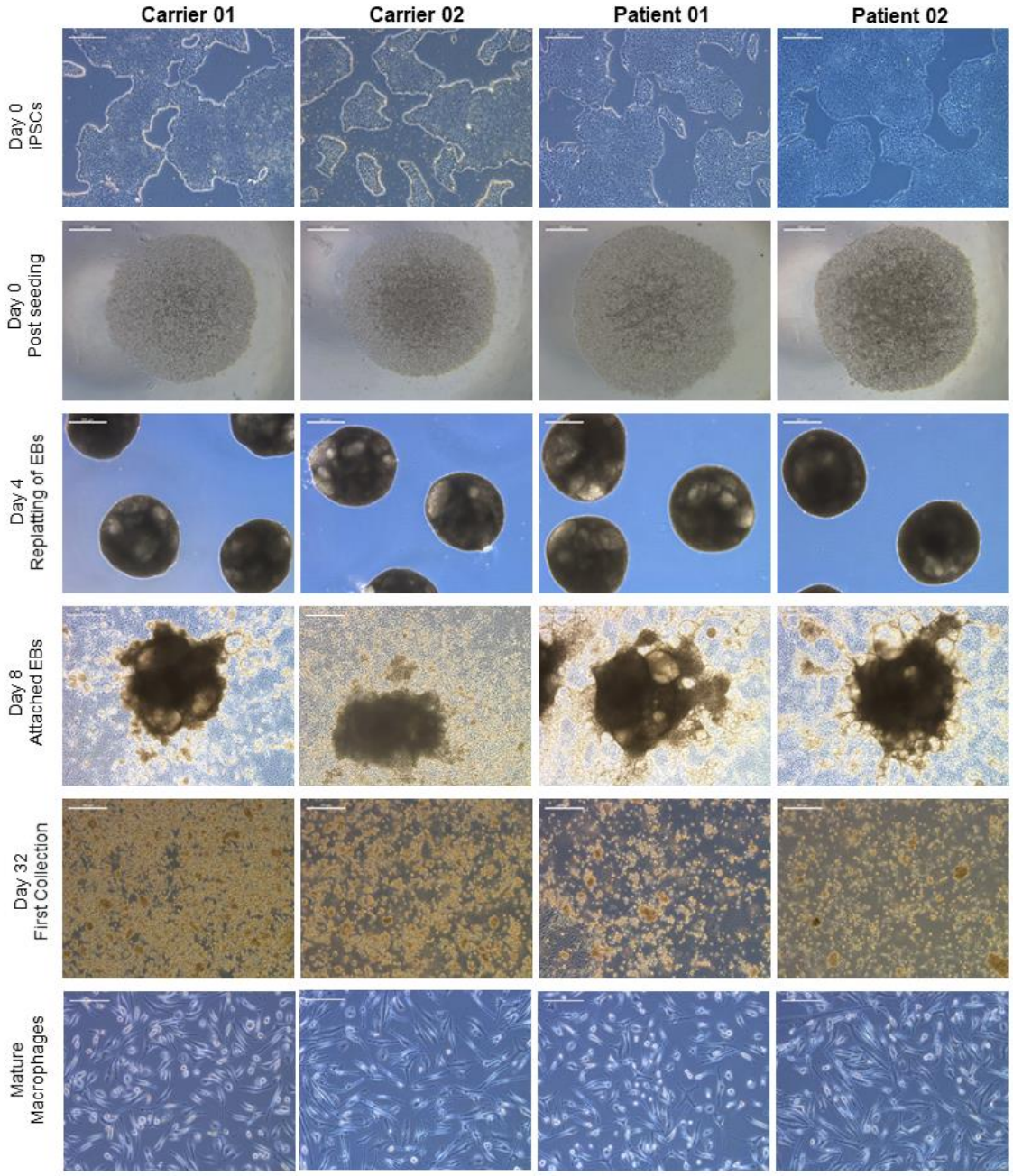

Figure 7- Representative images of initial phases of macrophage generation, from EB formation to differentiated macrophages. Images from day 0 to day 32 were taken with 4x magnification, scale bar: 500µm. Images from mature macrophages were taken with 10x magnification, scale bar: 200µm. All images were obtained with Inverted Microscope for Cell Culture DMi1 (Leica Microsystems).

4.2. Quality control and validation of macrophage generation

To verify cell identity and cell function, a quality control was performed. For cell identity, representative macrophage and hematopoietic lineage markers were tested and a phagocytosis functional assay was performed to verify macrophage's main function by flow cytometry.

4.2.1. Expression of characteristic surface markers

To access macrophage identity, flow cytometry was used. The gating strategy can be found in figure 8, consisting of doublet discrimination followed by selection of live cells.

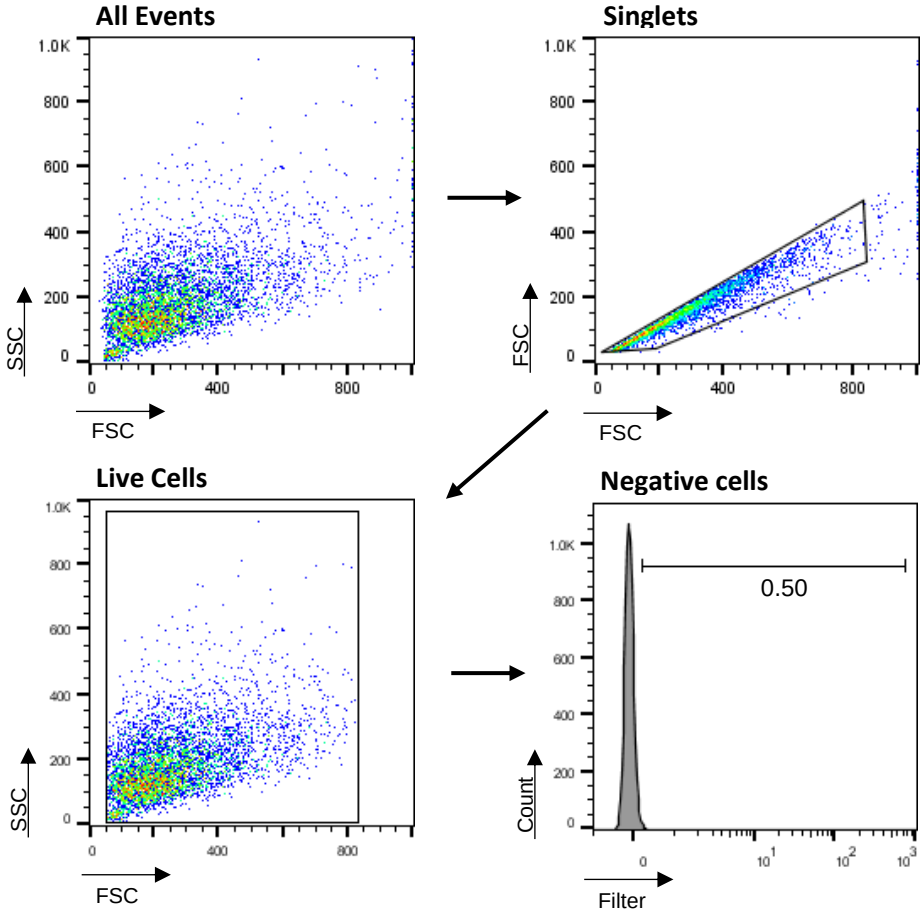

Figure 8- FlowJo plots demonstrating gating strategy for cell surface marker expression and phagocytosis measurement, the positive population is delimited by the bar. FCS-Forward scatter; SSC-side scatter.

Macrophages are highly plastic cells with a transient expression of markers. There is no specific macrophage surface marker so a panel of markers should be used. CD45 and CD14 were selected to confirm its myeloid identity whereas CD68, CD163 and CD86 are typical matured macrophage markers and were used for further validation and characterization (Lim et al., 2013). CD68 is present in most of tissue resident macrophages and is considered a classical macrophage marker (Chistiakov et al., 2017). Although its function is not completely elucidated, it is present in monocytes, particularly on LE, playing a role on the endocytic pathway by binding to oxidized LDL (Chistiakov et al., 2017). CD163, on another hand, is part of the scavenger receptor family, being mainly expressed in macrophages and present in most tissue resident macrophages subsets (Fabriek et al., 2009). It acts mainly in the process of clearance of circulating free Hb and as a receptor to bind gram-positive and gram-negative bacteria, modulating immune response (Fabriek et al., 2009). CD86 is characteristically expressed in antigen presenting cells, along with CD80, a receptor for the ligand CD28 that typically induces a pro-inflammatory response (Trombetta et al., 2018).

In figure 9, we can observe that most markers are present in a very high percentage of cells with an average of 99.48%±0.00200 for CD14, 99.13%±0.0078 for CD45, 97.30%±0.00889 for CD68 and 99.60%±0.00218 for CD163, confirming targeted cell identity. CD86, in contrast, with an average of 67.80%±0.150 is an exception, presenting lower values in iMph patient lines. The reason for this discrepancy is not quite clear. No other chemical stimulus besides M-CSF is used, however, batch effect, physical conditions of the culture, undefined serum formulation and handling for sample preparation are aspects that can have an impact on the macrophages activation status as they easily shift and express various markers in response to different environmental stimulus (Zhou et al., 2014). Having this in mind we can say that we have successfully differentiated precursor cells into mature macrophages, however its inflammatory status can be heterogeneous. Such aspect calls for further characterization of the model in terms of cell activation stages in response to external cues.

Table 6- Percentage of positive cell for each surface marker, along with the average positive cells± Standard Error.

iMph line

Surface Marker	C01	C02	P01	P02	Average ± Std. Error (SE)
CD14+	99.9%	99.5%	99.1%	99.4%	99.48% ±0.00200
CD45+	99.9%	99.7%	97.1%	99.8%	99.13% ±0.00781
CD68+	98.1%	95.3%	98.6%	97.2%	97.30% ±0.00889
CD86+	85.3%	89.3%	35.3%	61.3%	67.80% ±0.150
CD163+	99.9%	99.8%	99.1%	99.6%	99.60% ±0.00218

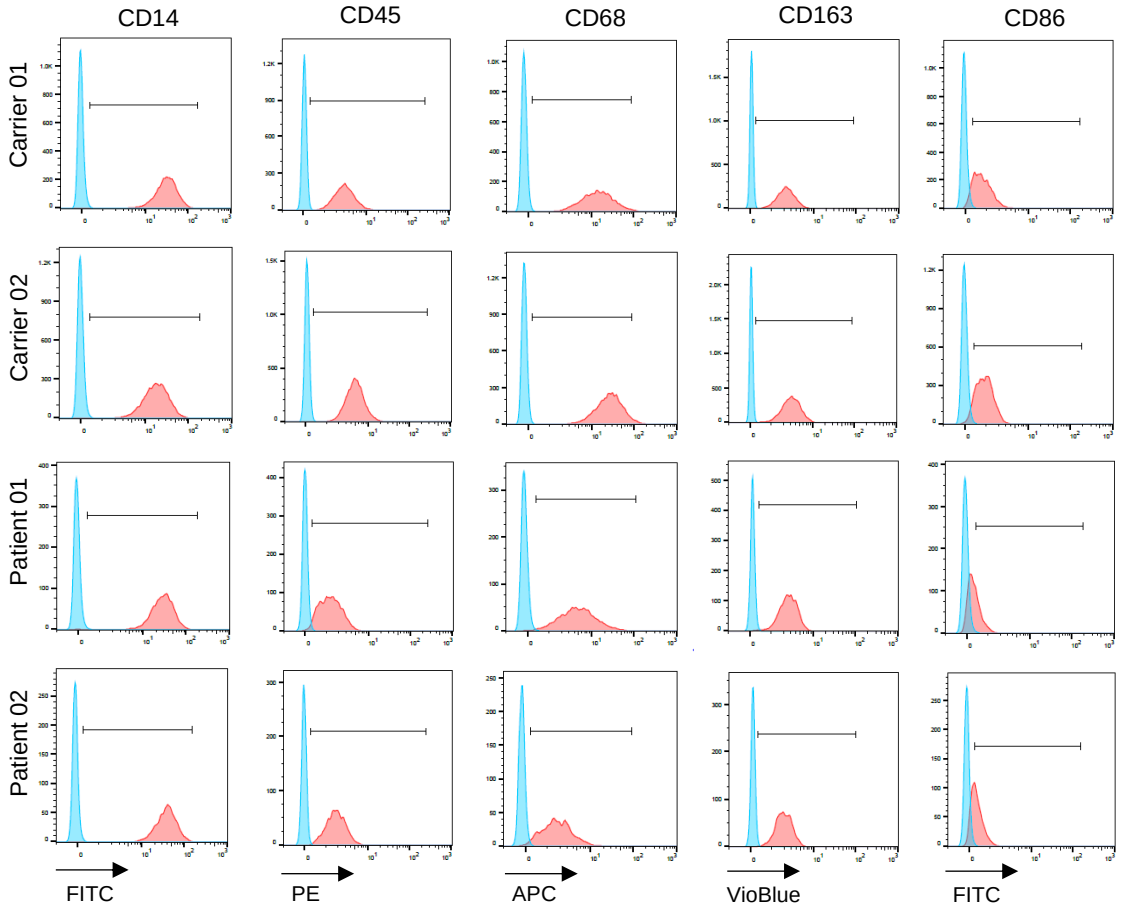

Figure 9- FlowJo plots of graphical representation of each surface marker in each sample. Stained samples are depicted in red and control samples are depicted in blue. The positive population is delimited by the bar.

4.2.2. Phagocytic capability

Macrophages by nature are phagocytic cells. This is one of their main biological functions, therefore it is important to evaluate this parameter to ensure the functionality of the model (Paul et al., 2013).

Studies regarding phagocytosis have shown that it is dependent on bead size, surface (polarity), amount, as well as temperature. Gu et al. (2014) reported the use of Carboxylated latex beads of 1µm diameter together with high uptake rates in macrophage cells. Based on that, the same conditions were tested in our iMph. Temperature wise, studies show that phagocytosis is more efficient under temperatures between 37º and 40ºC, with lowest uptake rates at 4ºC (Gu et al., 2014). Using the gating strategy previously presented, figure 10 shows an increase in cell complexity (SSC-A) after incubation with latex beads, suggesting the occurrence of particle internalization.

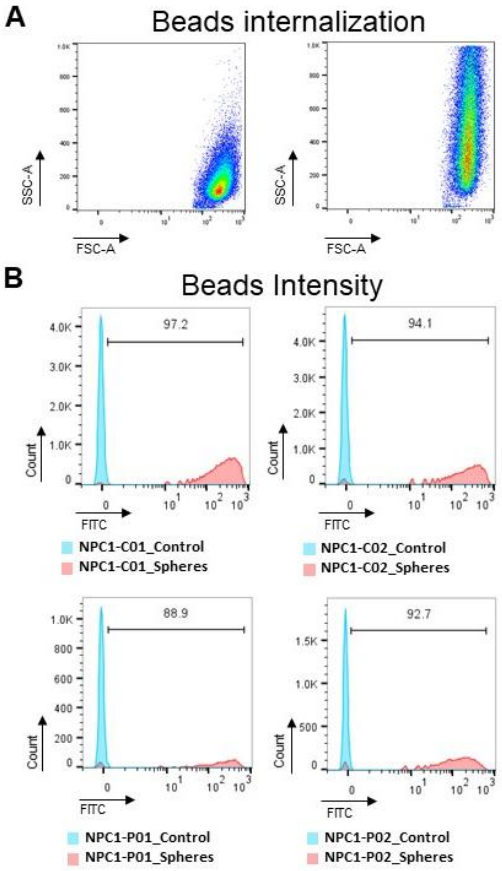

Figure 10- iMph were incubated with carboxylated latex beads with fluorescence for FITC channel. (A) Dot plot with all events in control and samples incubated with spheres (B) After exclusion of doublets and debris, the percentage of iMph positive for bead uptake was identified. average of 93.2% (SE±0.0210). Samples incubated with spheres are depicted in red and control samples are depicted in blue. FSC-A, forward scatter-Area; SSC-A, side scatter-Area.

Concomitantly, after the incubation with FITC-labelled beads, an average of 93.2% (SE±0.0210) of the cells were FITC positive, an indication of a population highly rich in phagocytic cells.

Macrophages are capable of performing other particle internalization processes besides phagocytosis, such as endocytosis, pinocytosis, macropinocytosis, and others (Lunov et al., 2011). To increase the degree of trust in the assay, uptake inhibitors can be used to inhibit other mechanisms to make sure the uptake of particles is being done through phagocytosis. From the get-go, using particles of 1um, as it is the case, excludes endocytosis as it can uptake particles of a maximum of 120nm of diameter. Macropinocytosis can be inhibited with rottlerin, pinocytosis with colchicine, monodansyl cadaverine for clathrin-mediated endocytosis, nystatin for caveolae mediated endocytosis and dynasore for dynamin dependent endocytosis (Lunov et al., 2011).

Overall, we not only verified this protocol's capability to robustly generate high cell yield with potential application in high throughput studies but also characterized such cells as functional macrophages. As a following step, it is important to confirm its relevance as a reliable model for NPCD and to assess the presence of key phenotypic features.

4.2.3. NPC1 and LAMP2 proteins immunocytochemistry

To confirm NPCD phenotype in the generated model, we begin by evaluating the presence or absence of NPC1 protein along with LAMP2, a lysosome associated membrane protein (LAMP), in the two carrier lines and one patient by fluorescence microscopy. LAMP2 allows the study of the subcellular localization of lysosomes as they are major components of the lysosomal membrane (Eskelinen, 2006).

Quantification was taken ahead with a custom quantification module. Through use of a cell mask and nuclear marker two binary masks were build that segment and show the contour of each individual cell. Border objects were removed, and the average NPC1 and LAMP2 signal intensity was measured.

In figure 11, we can visualize and assess through intensity quantification of NPC1 protein that iMph Patient 01 presents a drastically lower intensity, with an average intensity of 863.2±4.829 comparing with 1844±13.97 and 2463±14.87 for carrier 01 and carrier 02, respectively. This indicates a lower expression and presence of the protein in

the cells which is aligned with the mutation in question. On the other hand, LAMP2 signal was the highest in the patient iMph rather than carriers with an average intensity of 3858±37.95 against 3208±33.78 and 2742±17.85 for carrier 01 and carrier 02, respectively. This can be due to the defective endocytic trafficking already reported in

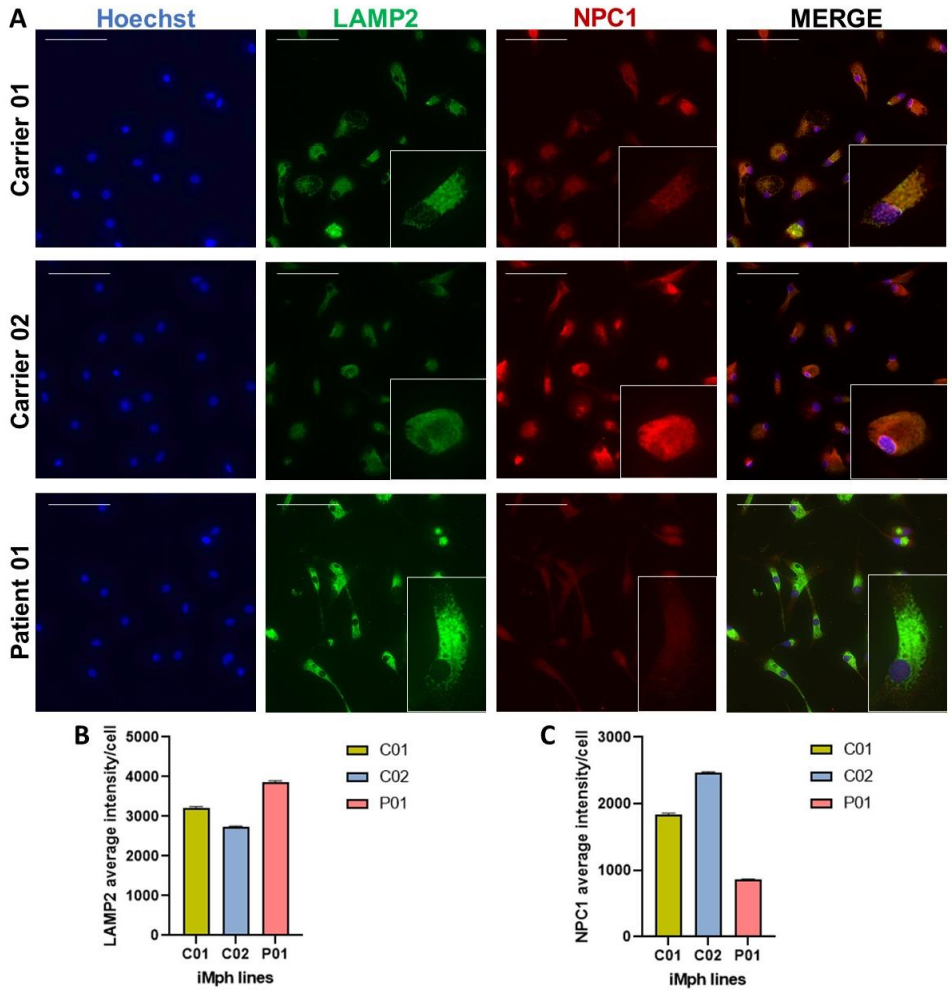

Figure 11- (A) Fluorescence microscopy of patient and carriers iMph using anti-NPC1 (red) and anti-LAMP2(green) antibodies, 40x with zoom. Scale bar:100µm. (B) Average LAMP2 signal intensity per cell. (C) Average NPC1 signal intensity per cell. Differences between groups were evaluated using the Kruskal-Wallis test with original FDR method of Benjamini and Hochberg for multiple hypothesis testing correction, pair-wise comparisons gave statistically significant differences between all groups with and individual p-value lower than 0.0001. For C01, n=3391; C02, n=6905; P01, n=3306.

NPC1 patients (Colaco et al., 2020). For instance, Sarkar et al. (2013) observed an increase in LAMP1, akin to LAMP2, in NPC1$^{-/-}$ mouse embryonic fibroblasts suggesting the occurrence of lysosomal accumulation in the cytoplasm.

It could be expected that the heterozygous iMph lines would show no significant differences between them, however the carrier 01 iMph shows intensity values for both NPC1 and LAMP2 protein in between of those found in patient 01 and carrier 02, showing lower levels of NPC1 and higher levels of LAMP2 in comparison with carrier 02. However, there are reports of carriers of NPC1 presenting some type of phenotype already dating back to 1988 and this can be such a case (Vanier, 2010). Vanier et al evaluated the esterification capacity of LDL-derived cholesterol and found 9 of the 21 obligate heterozygous showed intermediate values (Vanier' et al., 1988). Later, Vanier et al. not only verified intermediate esterification levels of cholesterol, but also, storage of abnormally high levels of unesterified cholesterol (Vanier et al., 1991). Having confirmed the low levels of NPC1 protein in the iMph patient lines in comparison with carrier ones, we next assessed the impact of such differences on iMph, particularly in terms of cholesterol transport.

4.2.4. Presence of cholesterol

Accumulation of intracellular cholesterol is one of the most important hallmarks of NPC1 and a direct result from the impaired function or lack of NPC1 protein. Evaluation of cholesterol content was performed by fluorescence microscopy through Filipin staining. Quantification was taken ahead with a custom quantification module that followed the strategy presented in figure 12, in accordance with other published strategies (Wilhelm et al., 2019).

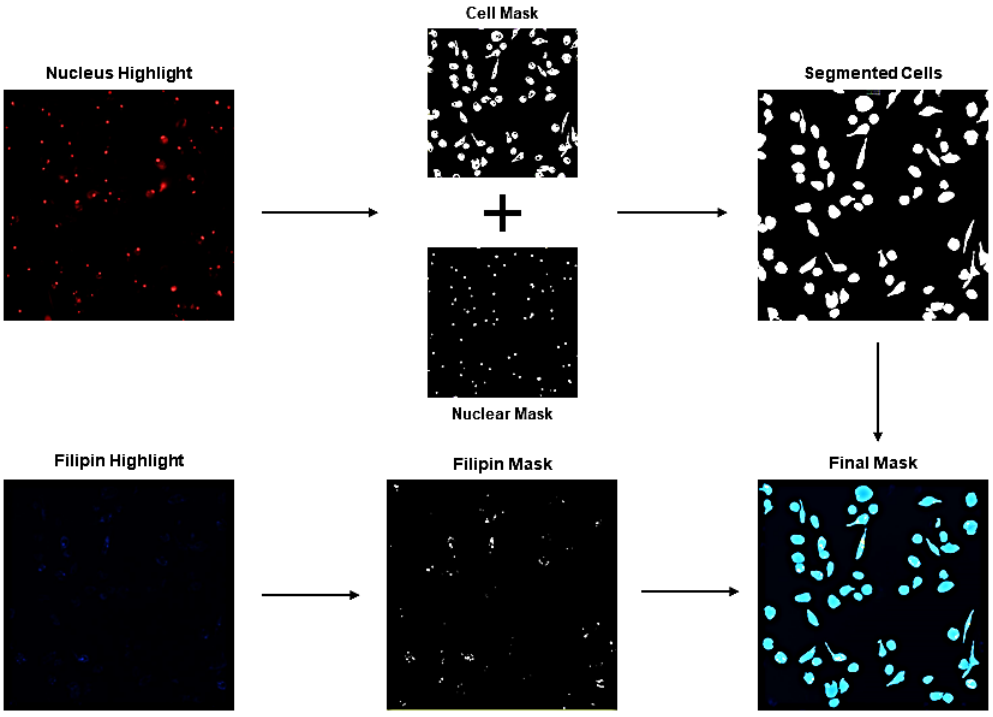

Figure 12- Segmentation strategy to measure filipin positive cells. A fluorescence threshold was applied to highlight the nucleus and the cell outline. These images were combined to segment the cells and show the contour of each individual cell. Filipin vesicles were highlighted based on pixel shape and size, then the width and intensity dimensions above the local background were set to create a Filipin mask used to calculate average vesicle area.

In figure 13, both in the microscopy images and the filipin quantification plot, we can observe a significant difference in cholesterol accumulation between heterozygous and homozygous iMph. Large vesicles positive for filipin were detected in homozygous lines, a result consistent with what was observed in macrophages under cholesterol transport inhibition (Huynh et al., 2008). Patient's iMph presented an average filipin area of 16.95µm^2±0.3232 and 12.49µm^2±0.3489 for patient 01 and patient 02, respectively. Meanwhile, carrier's iMph presented an average filipin area of 0.7226µm^2±0.06383 and 0.3984µm^2±0.04290 for carrier 01 and carrier 02, respectively.

Furthermore, to further validate filipin reliability and specificity for cholesterol, Nile Red staining was performed. It has been extensively used to stain lipid droplets, phospholipid monolayered vesicles with an enriched core of neutral lipids that provides and stores lipids as necessary, however it loses some of its specificity when excited above 560nm of wavelength, staining almost every lipid in the cell, including cholesterol (Greenspan et al., 1985; Olzmann & Carvalho, 2019). As we can see in figure 13, there

is a significant but not complete overlap indicating that, as expected, filipin is more specific staining only free cholesterol.

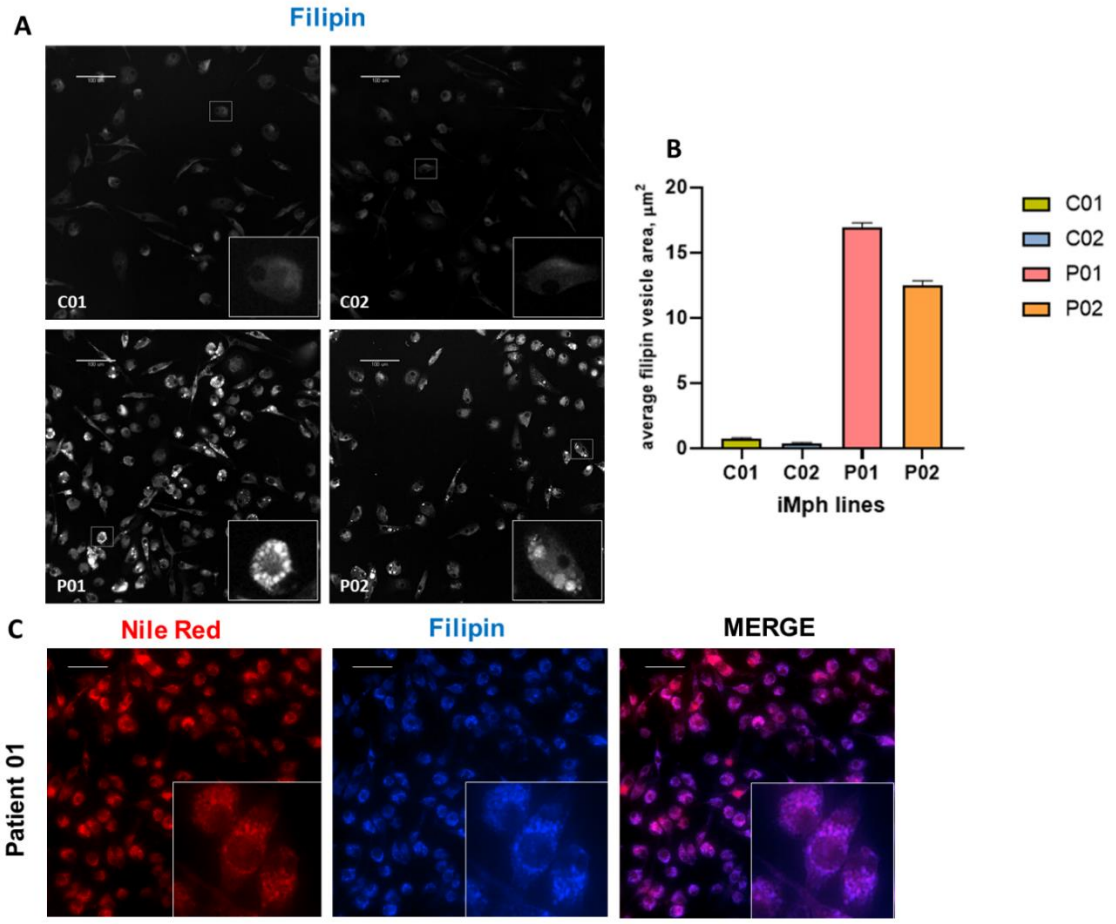

Figure 13- (A) Fluorescence microscopy of patients and carriers iMph for filipin staining, 20x with zoom. (B) Average vesicle area of filipin with SEM. Kruskal-Wallis Test was performed to access differences between groups, all groups were statistically different (p.value<0.0001, except C01-C02, p.value<0.0055). For C01, n=8265; C02, n=7239; P01, n=7537; P02, n=4018. (C) Fluorescence microscopy of patient 01 iMph for filipin and nile red, with some apparent co-localization in the merged image, 20x. Scale bar:100µm.

In an attempt to look deeper into the nature of these filipin positive vesicles, a co-staining with LAMP1 and LAMP2 was performed. In the merged image we can see that there is a high degree of overlap between filipin-positive vesicles and LAMP1/LAMP2 signal, suggesting an accumulation of free cholesterol within lysosomes, therefore validating the presence of one of the main hallmarks of the disease in the developed model.

We also co-stained for Perilipin-2, part of the perilipin family of proteins that is localized in the membrane of lipid droplets involved in lysosome-lipid droplet interactions, therefore allowing for its specific detection. As mentioned, lipid droplets at its core possess mainly neutral lipids, thus presence of free cholesterol is not expected. Some work has revealed that this can vary in cells like Hepatic stellate cells, indicating that the composition of lipid droplets may differ according to cell type (Blaner et al., 2009; Onal et al., 2017). In our findings, no significant overlap of perilipin-2 with filipin positive vesicles is observed in figure 14, suggesting that there is no accumulation of free cholesterol in lipid droplets of macrophages.

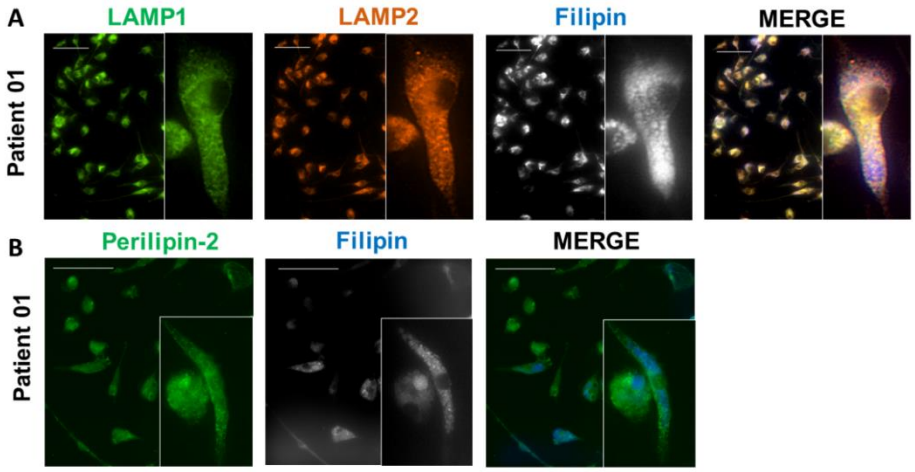

Figure 14- (A) Fluorescence microscopy of patient 01 iMph using anti- LAMP1 (green) and anti-LAMP2 (orange) antibodies, and filipin staining (black and white) 20x with zoom. (B) Fluorescence microscopy of patient 01 iMph using anti-perilipin-2 (green) and filipin staining (black and white) 20x with zoom. Scale bar: 100µm.

Although no staining was performed for LAMP1 negative late endosomes, accumulation of free cholesterol in late endosomes has been reported and has been mentioned earlier in this work. Therefore, it is likely that they constitute the remaining filipin-positive vesicles observed in patient lines. Endocytic pathway is regulated by the Rab family of proteins and the transition from early endosomes to late endosomes is accompanied by “Rab conversion”, i.e, association by Rab5 is switched to association by Rab7 (Hu et al., 2015). As future work, a co-staining with Rab7 protein could be useful to further characterize the nature of the filipin positive vesicles observed in the developed NPCD iMph model.

Aligned with the results obtained for NPC1 and LAMP2 immunocytochemistry where iMph carrier's 01 presented some abnormality, we can observe some sparce small-sized filipin vesicles which is backed up by the existence of statistically significant differences between both carriers iMph.

As previously referred, one of the main challenges for the treatment and study is the usual non-translation between genotype and phenotype, siblings with the same mutation can have different phenotypes, making it hard to predict the severity of the disease by the mutation in question (Pallottini & Pfrieger, 2020). In our case, the degree of free cholesterol in NPCD iMph seems to be aligned with the level of disease severity of the patient. In figure 13, we can see that patient 01 presents more cholesterol accumulation than patient 02 as showed by filipin vesicle area quantification.

Patient 01 presented a frameshift mutation with a PTC and a change from proline to arginine in position 543 of the protein. In fact, a study by Macías-Vidal and colleagues evaluated 11 NPC1 mutations encoding at least one PTC and observed the occurrence of mRNA decay (Macías-Vidal et al., 2009). Accordingly, it is possible that in our case such change results in mRNA degradation through Nonsense-mediated mRNA decay, which would corroborate the fact that this patient presents the most severe phenotype. On another hand, patient 02 has a missense substitution leading to a tyrosine instead of a cysteine. It is known that cysteine has a sulfhydryl group which allows the formation of disulphide bonds that are extremely important for correct three-dimensional protein conformation (Wiedemann et al., 2020). Considering this, its exchange for tyrosine that has an aromatic group instead, likely leads to a misfolded protein which is not fully functional or may be marked by degradation in the proteasome, not reaching the lysosome.

In summary we were able to confirm that the cellular model shows one of the main hallmarks of NPC phenotype, the accumulation of non-esterified cholesterol in lysosomes, and to ascertain that different NPC1 mutations show different levels of cholesterol accumulation to the point of being statistically significant. Furthermore, by combining cholesterol accumulation and lysosomal content as read-out, iMph seem like a reliable model in the context of NPD with potential for application in high throughput compound testing.

4.3. Macrophage Polarization

As a macrophage, polarization potential its key in fulfilling their functions. If a macrophage is not able to shift and change in accordance with different stimuli, they are not functional (Funes et al., 2018). Therefore, it is important to validate iMph model's polarization potential. To that end, both patient and carriers iMph were stimulated with GM-CSF and IFN-γ to induce a M1 state or M-CSF and IL-4 for a M2 state. Morphology assessment and RNA-sequencing of induced iMph was performed, allowing simultaneous evaluation of both polarization status as well as relevant pathways and potential targets in NPC1.

4.3.1. Morphology

Stimulation of M0 iMph into M1 and M2 iMph subsets induced morphologic alterations. Polarization into an M1 phenotype through the use of IFN-γ and GM-SCF resulted in a change in morphology from typically elongated cells to a more circular amoeboid shape that was quite distinct. On the other hand, the polarization to an M2 phenotype with the use of IL-4 and M-CSF resulted in equally elongated but more expanded, irregular and flat cells with increased number of processes. Phase contrast images can be found in figure 15. Polarization into different inflammatory phenotypes induced markedly different morphologies, as it has been reported before (G. Hu et al., 2021; Rostam et al., 2017). McWhorter et al (2013) studied the effect of cell morphology and it's changes according to their inflammatory phenotype, finding a strong link between the two. By micropatterning macrophages into inducing an elongated shape, they showed that it led to the expression of key M2 phenotypic features such as an increase in arginase-1, CD206 and YM-1 coupled with a reduction in pro-inflammatory cytokine production suggesting that cell shape synergizes with cytokines in M2 polarization (McWhorter et al., 2013).

Hence, cell shape is valid characteristic to assess a macrophage's polarization status for M1 and M2, visually showing the great plastic ability of macrophages to respond to external stimuli and indicating a successful polarization of the model, which led us to proceed with the study of its transcriptome (Hu et al., 2021).

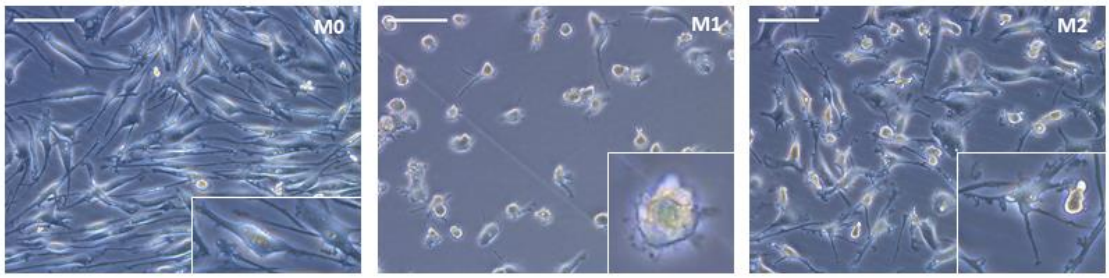

Figure 15- Representative images of cell morphology for M0 (M-CSF), M1 (IFN-γ+GM-CSF) and M2 (IL-4+M-CSF) activated macrophages, 20x. Scale bar: 100µm. All images were obtained with Inverted Microscope for Cell Culture DMi1 (Leica Microsystems).

4.3.2. Transcriptomics

In table 7, the quality of the data can be inferred. We observe that the starting material had high quality with a very high Rin^e ranging from 8.4 to 9.8. The library generation was successful, as indicated by a consistent average size of the generated reads, with a high-quality rate and a considerable amount of mapped unique reads.

Table 7- Information regarding the quality of RNA-seq samples.

Polarization Status	Line	Sample	Rin^e	Conc. (ng/ul)	Average size (bp)	Quality Rate (%)	Mapped Unique reads	Exonic Rate (%)	%mRNA
M0	C 01	S1	9.6	28.2	335	97.5	43 387 706	84.1	86.9
		S2	9.5	16.8	338	97.5	52 341 856	84.5	86.4
		S3	9.6	25.9	328	97.3	40 744 764	81.5	83.7
	C 02	S4	9.0	16.6	324	97.4	46 758 741	85.3	88.2
		S5	9.4	23.1	338	97.4	44 905 641	85.4	87.8
		S6	9.3	15.5	341	97.5	44 738 814	85.3	88.0
	P 01	S7	9.4	28.1	335	97.4	46 651 449	84.5	86.8
		S8	9.6	19.6	335	97.4	41 539 203	85.3	87.0
		S9	9.5	19.4	341	97.4	40 350 028	85.4	87.0
	P 02	S10	9.4	14.5	332	97.2	50 924 090	84.8	86.4
		S11	9.6	12.5	334	97.3	44 466 491	86.3	87.7
		S12	9.6	11.5	345	97.3	43 287 171	84.7	85.8
M1	C 01	S13	9.3	16.0	345	97.6	39 627 343	84.6	89.1
		S14	9.2	15.5	351	97.6	45 247 632	84.4	89.0
		S15	9.3	19.0	342	97.5	41 625 251	82.9	87.4
	C 02	S16	8.7	23.2	336	97.5	42 752 326	85.1	88.6

		S17	8.8	29.9	337	97.5	49 533 811	84.9	89.3
		S18	9.1	18.8	335	97.6	43 894 054	84.5	88.7
	P 01	S19	9.1	20.5	322	97.3	43 600 840	84.8	88.3
		S20	9.1	25.2	357	97.5	42 986 958	85.0	89.1
		S21	9.6	29.3	338	97.4	40 975 476	85.0	88.8
	P 02	S22	8.9	33.1	344	97.5	41 869 744	84.7	88.9
		S23	9.5	32.0	327	97.3	47 436 430	85.0	88.7
		S24	8.9	27.4	327	97.3	45 345 345	84.5	88.1
M2	C 01	S25	9.8	17.7	346	97.5	42 622 426	85.1	87.0
		S26	9.8	9.80	336	97.6	40 188 319	85.8	87.7
		S27	9.6	11.7	352	97.7	41 984 796	85.2	86.7
	C 02	S28	9.1	11.1	355	97.7	37 738 878	86.1	87.7
		S29	9.4	15.3	342	97.7	37 823 035	86.1	88.0
		S30	9.7	8.89	351	97.7	42 548 288	84.1	85.2
	P 01	S31	9.7	19.0	334	97.1	39 840 881	85.9	86.3
		S32	9.6	15.3	339	97.1	39 678 207	85.9	86.5
		S33	9.6	15.6	329	97.1	41 675 370	86.4	86.8
	P 02	S34	9.5	13.8	331	97.3	45 947 668	83.7	84.7
		S35	9.6	23.5	332	97.2	47 120 265	85.6	87.4
		S36	8.4	21.2	339	97.2	46 826 046	85.1	86.6

4.3.2.1. Assessment of polarization potential

Genes were considered differentially expressed genes (DEG) with an absolute Log_2FC of >0.58 and <-0.58 and FDR p-value <0.05. In the principal component analysis (PCA) plot (figure 16) it is clear that the three groups are clustered separately, indicating that there are differences between them, particularly M1 that is evidently segregated, presenting high variance. M1 comparison with M0 macrophages resulted in 5317 DEG, from which 2995 genes were downregulated, and 2322 genes were upregulated. As far as M0 and M2, these presented 3783 DEG, from which 2102 genes were downregulated and 1681 were upregulated. We can see in the principal component analysis (PCA) plot that M2 polarization status doesn't seem to have induced such a dramatically different transcriptional profile, seeming to present some degree of similarity or a low level of variance comparing to M0.

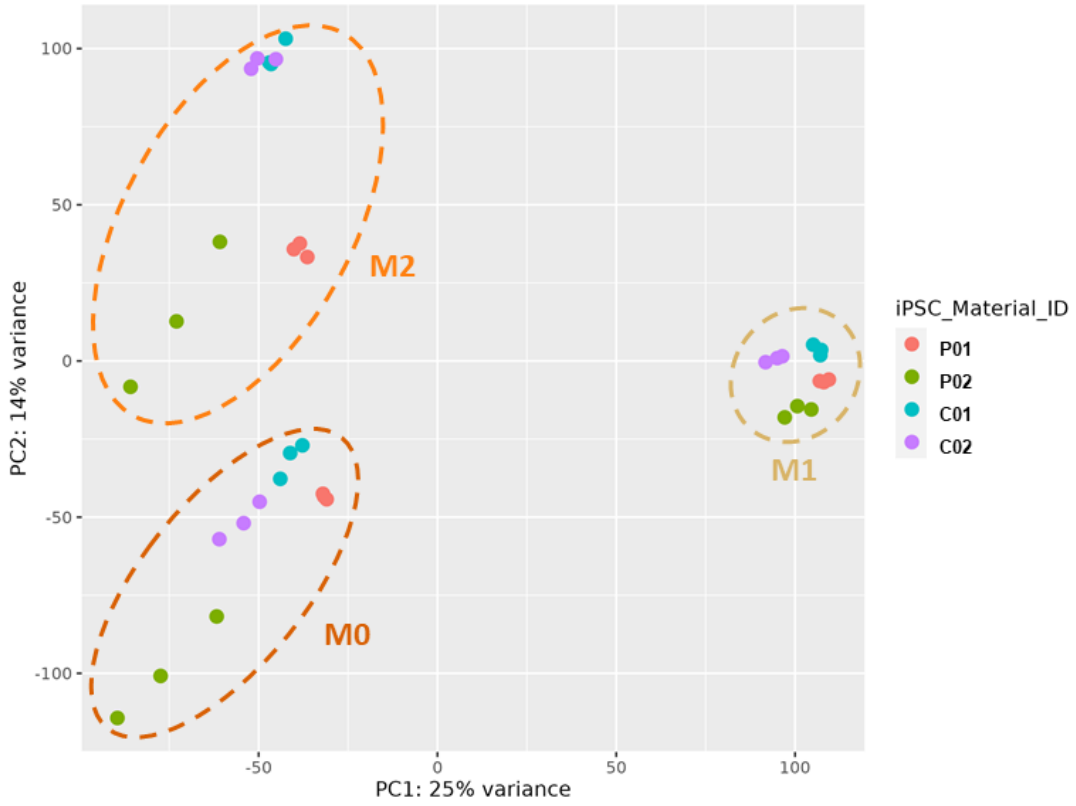

Figure 16- Principal component analysis of all samples. It was generated using the normalized count matrix by DESeq2 and submitted to the R function 'prcomp'. The plot was kindly provided by the Bioinformatics department.

When comparing heterozygous and homozygous samples in M1, both disease and carriers cluster together, indicating that there are no striking differences between them. As far as M0 and M2, both groups P02 triplicates presented some variance between them, not clustering together. From the three groups, M2 samples is the one polarization status that shows a clear difference between homozygous and heterozygous samples.

Subsequently, we evaluated the activation status of IFN-γ and IL-4 pathways to assess if these were successfully activated. In IPA, differential expressed genes from heterozygous samples were overlaid with the existing pathways in IPA's repository, IFN signalling for M1 dataset and IL-4 signalling for M2 dataset. We can see a clear activation of the IFN-γ pathway in M1 polarized iMph as indicated by the clear upregulation of both JAK-STAT pathway and SOCS1, which mediates feedback inhibition when under high doses of IFN-γ (X. Hu et al., 2008). The activation of this key pathway indicates a successful polarization of iMph and their shift into a pro-inflammatory phenotype.

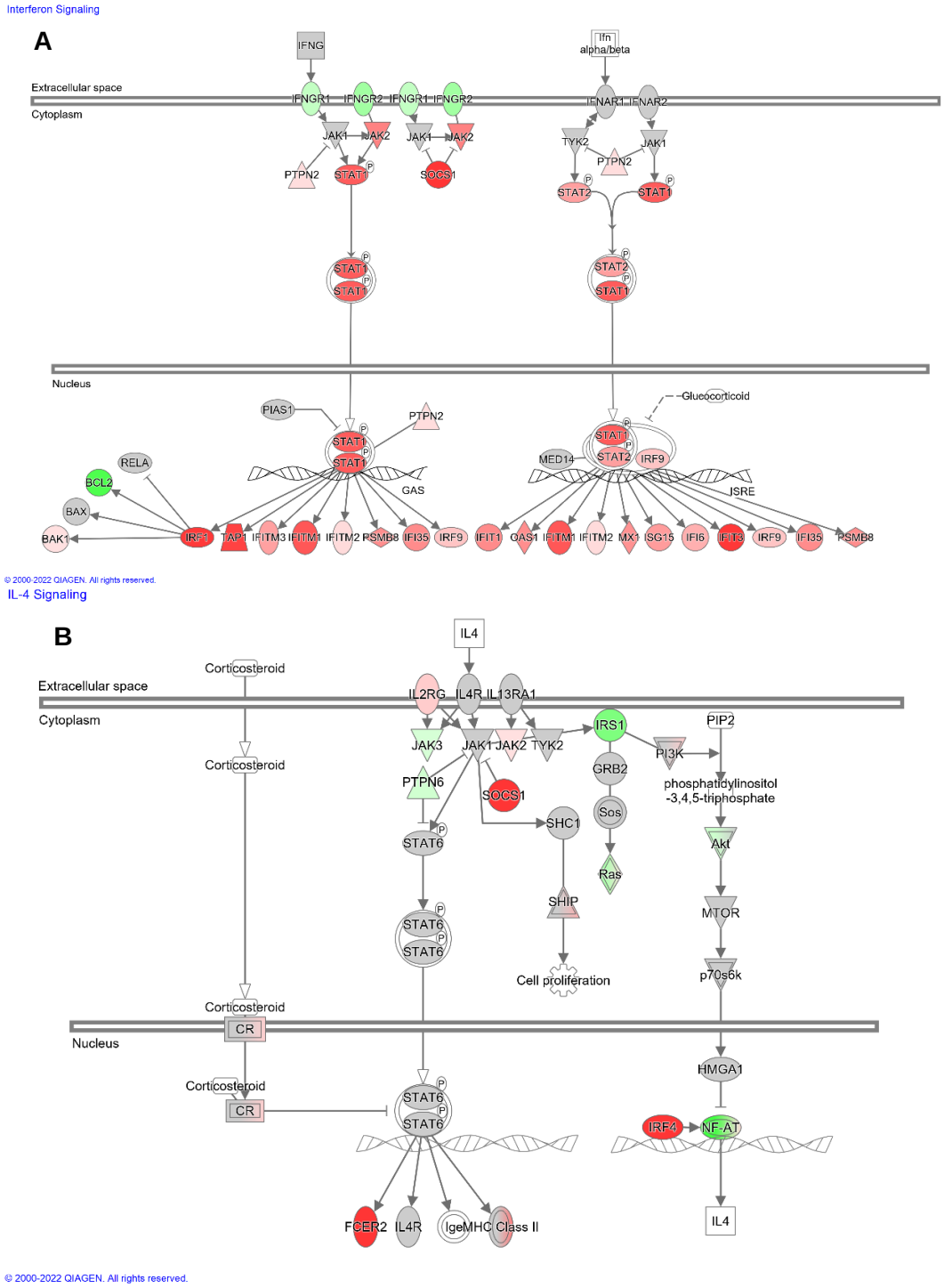

Figure 17- (A) Interferon signaling pathway overlaid with DEG genes from M1 heterozygous samples dataset. (B) IL-4 signaling pathway overlaid with DEG genes from M2 heterozygous dataset. Absolute Log2FC of >0.58 and -0.58< and FDR p-value <0.05 was considered differentially expressed. Red range of colours shows upregulated genes, green range of colours shows downregulated genes and grey shows non-affected genes. IPA software (Qiagen, all rights reserved) licensed to Centogene.

On other hand, results show a downregulation in IFNGR1 and IFNGR2.

Accordingly, Wang et al (2008) described a negative feedback mechanism by IFN-γ, by inducing expression of IRF-2 which in return negatively regulates IFNGR1 on oesophageal squamous cell carcinomas (Wang et al., 2008). More recently, Crisler et al. (2019) reported a suppression of IFNGR1 transcripts upon IFN-γ exposure on murine macrophages, resulting in a refractory response in subsequent exposure (Crisler et al., 2019). Overall our results are in alignment with these reports as we observe a decreased expression of both IFNGR1 and IFNGR2 in response to exposure of long-term and high-concentration of IFN-γ.

In regard to M2 dataset, the results are not as straightforward as we do not observe a clear upregulation of the classical elements of the pathway. This led us with the question – wasn't the polarization successful? Such hypothesis seemed highly unlikely as IL-4 is a well-known inducer of M2 macrophages and IFN-γ results demonstrated that the model is susceptible to polarization in some way (Wynn et al., 2013). To answer that question, it is required to look at a broader transcriptomic profile of the cells under such conditions. Therefore, a heatmap with expression z-scores for a selection of representative genes of M1 and M2 macrophages was generated.

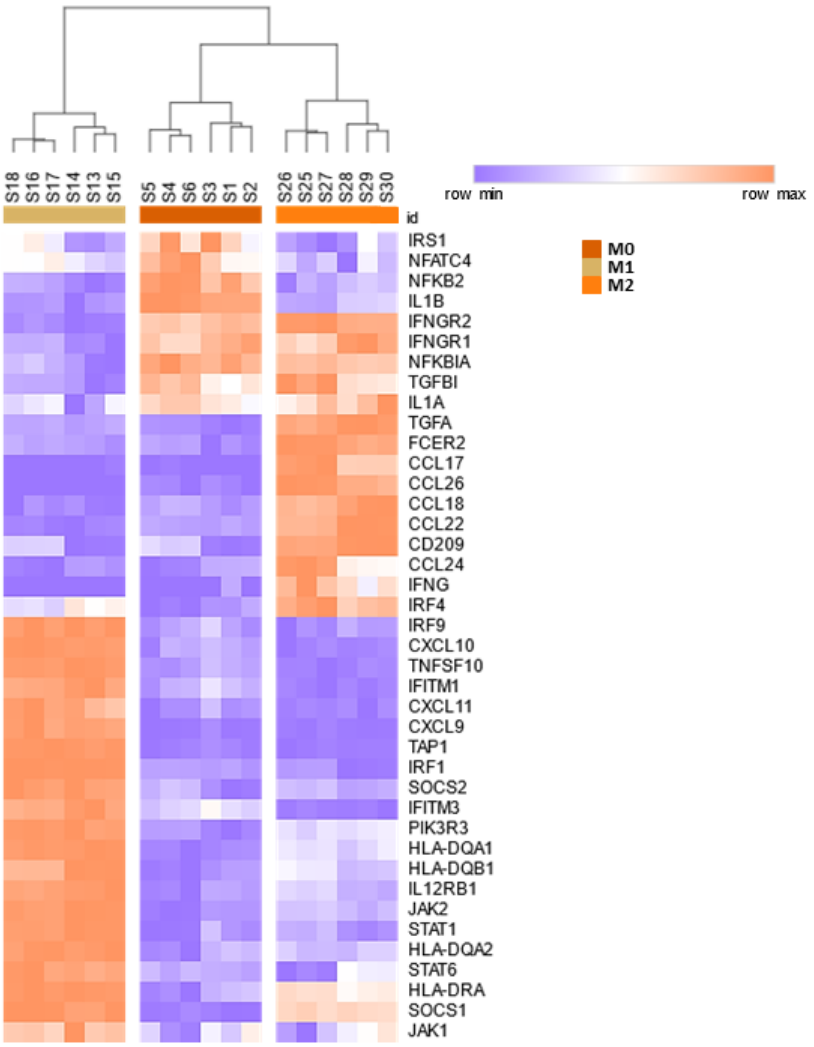

Figure 18- Heatmap comparing representative genes for M1 and M2 polarization. Expression values are depicted in z-scores with the colour bright orange representing the maximum value and bright purple representing the lowest score for each gene. Heatmap was obtained in Morpheus online tool by Broad institute with euclidean clustering.

Based on the heatmap (figure 18) we can perceive that even though components of IL-4 signalling pathway are not upregulated, typical M2 chemokines such as CCL18 and CCL22 are. This suggests that IL-4 induction resulted in cell activation and transition to a more anti-inflammatory state, detectable in their transcriptional profile. Additionally, Gerrick et al (2018) found that M2 polarization with IL-4 and IL-13 in blood derived monocytes obtained from whole blood samples resulted in lack of expression of IL-10 and CCL17, important cytokines in this subset, which were rescued by co-stimulation with LPS (Gerrick et al., 2018). In contrast, our iMph presented a $\log_2$FC of 14.9 and 0.70 for CCL17 and IL-10, respectively. The fold change of CCL17 is very high indicating that

indeed it is extremely upregulated, IL-10 not as much, but still significantly upregulated. This could be due to the adopted method to generate macrophages, which can be used as a positive argument for iMph and something to have in mind when modelling macrophage-based disease models.

Considering that, it is still questionable why a clear activation of IL-4 signalling pathway is not detectable and why M0 and M2 do not present major differences at a transcriptional level as it is suggested by the PCA plot. A possibility is that what we consider M0 iMph may in fact present more similarities with M2 iMph than initially expected. Interestingly, Martinez et al (2006) reported that polarization into a M1 phenotype induced a major shift in the transcriptional profiles of macrophages and minor, yet significant shift in M2 polarization (Martinez et al., 2006). Our results are in alignment with such findings with one of the hypotheses for this similarity between M0 and M2 being the common M-CSF driven differentiation (Martinez et al., 2006). This is supported by the idea that M-CSF is expressed constitutively in tissues under homeostatic conditions and is reported to promote an anti-inflammatory phenotype in macrophages. On the other hand, GM-CSF is mainly produced in response to a stimulus, such as infection or injury, promoting a pro-inflammatory response (Lacey et al., 2012; Martinez et al., 2006; Ushach & Zlotnik, 2016). Therefore, indicating that M0 macrophages may be considered M2-like and M2 might be a default state in macrophage differentiation as result of the addition of M-CSF (Martinez et al., 2006; Orekhov et al., 2019).

In sum, the generated model presents the typical macrophage plasticity required to attain the two most common polarization status, M1 (induced by GM-CSF and IFN-γ) and M2 (induced by M-CSF and IL-4). While M1 induced a drastic shift in transcriptional profile, M2 induced only a minor shift, suggesting a similarity with the M0 state.

4.3.2.2. Heterozygous *versus* Homozygous

Having described the model's features and reliability to be used in the NPCD context, we performed an initial assessment of the potential transcriptomic differences between homozygous and heterozygous samples. From the get-go, although in the PCA plot there wasn't high variance between heterozygous and homozygous, the DEG with Log_2FC of >0.58 and <-0.58 and FDR p-value <0.05 were analysed on KEGG Pathway Database (Kanehisa Laboratories). From some of the main pathways involved in NPCD such as sphingolipid metabolism, lysosomes, autophagy and inflammation, a selection

of genes were retrieved with potential role in the disease. Those were selected for further analysis.

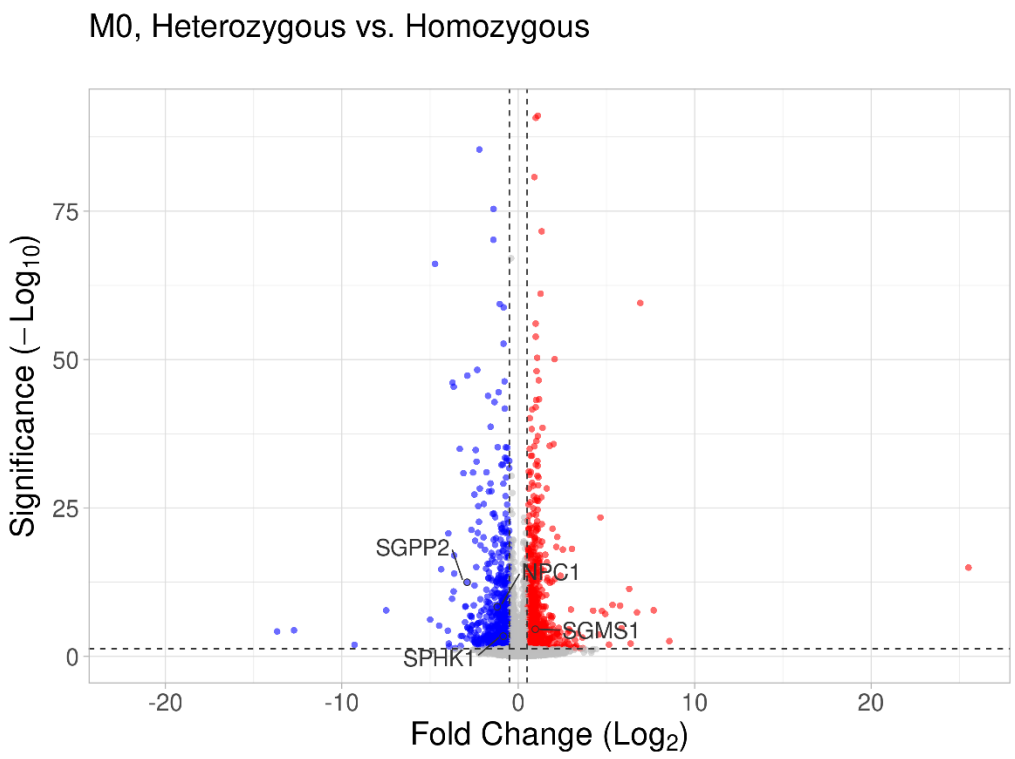

Figure 19- Volcano plot of heterozygous versus homozygous for M0 samples. The red dots represent up-regulated genes, the blue ones represent down-regulated genes, and the gray ones are either not affected or no significance.The red dots represent up-regulated genes, the blue ones represent down-regulated genes, and the gray ones are either not affected or no significance. Volcano plot was obtained with *VolcaNoseR* (Goedhart and Luijsterburg, 2020).

In M0 samples a total of 1338 DEG were found, from which 750 genes were up-regulated and 588 were down-regulated. The genes that emerged as disease relevant were SGPP2 (Sphingosine-1-Phosphate Phosphatase 2), SGMS1 (Sphingomyelin Synthase 1), SPHK1 (Sphingosine Kinase 1) and NPC1 which are mainly involved in sphingolipid metabolism (figure 20).

SPHK1, phosphorylates sphingosine (SP) into Sphingosine-1-Phosphate (S1P) which is involved in a cascade of events that lead to degradation of complex sphingolipids.(Newton et al., 2020) It is also a key regulator of cellular processes such as survival, proliferation, differentiation and migration in the brain, which is important to note since NPC1 has a very significant neurological component. Interestingly, a major hypothesis for the accumulation of sphingosine in the lysosome is the impairment of

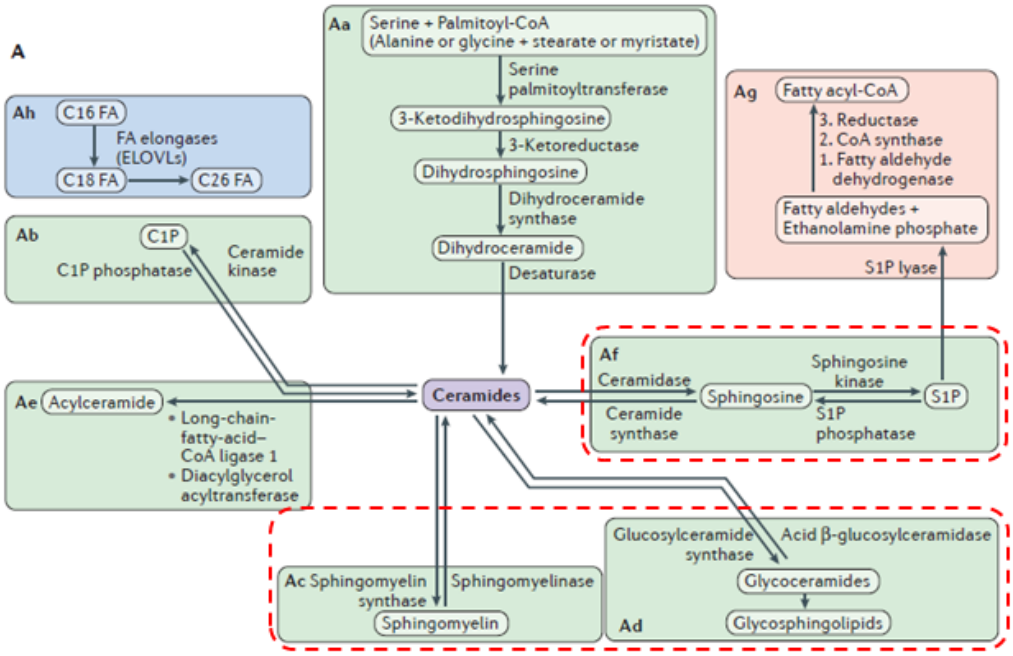

Figure 20- Overview of Sphingolipid metabolism, the most relevant pathways for NPCD are highlighted in red. Adapted from Hannun & Obeid, 2018.

SPHK1/2 enzymes that perform its conversion to S1P and allow its release from the lysosome (Newton, Milstien, and Spiegel 2018). Accordingly, Gläser et al (2020) evaluated accumulation of several lipids in different areas of the brain of sham-treated NPC1$^{-/-}$ mice, having found accumulation of sphingomyelin, sphingosine and a decrease in S1P (Gläser et al., 2020). Moreover, a report from Newton et al (2020) showed reduced SPHK1 activity in NPC1 mutant fibroblasts which was rescued by its activation with SK1-A, leading to decrease accumulation of free cholesterol and restoring cholesterol egress (Newton et al., 2020). Overall, the literature findings are corroborated by our dataset were we observe a slight downregulation in SPHK1, which can play a role in sphingosine accumulation and subsequent lack of S1P in NPC1 cells.

SGPP2 mediates the degradation of S1P by its dephosphorylation into sphingosine (Hannun and Obeid, 2018). This gene is significantly downregulated, and one could think that it can be a cellular protective mechanism to cope with sphingosine accumulation. On the other hand, SGMS1 catalyzes conversion of ceramide into sphingomyelin, a lipid that also suffers accumulation in NPC1 (Hannun & Obeid, 2018). In this dataset, we can observe upregulation of the gene. Contrarily to SPHK1, no studies

were found in regard to modulating SGPP2 and SGMS1 function in NPC1, neither were these approached in the only single cell RNA-seq study on NPC1 cells (Cougnoux et al., 2020).

Interestingly enough, we detected a difference in LAMP2 average intensity when comparing carriers and patient 01 in immunostainings, however no significant differences were observed at a transcriptomic level. This means that there is no significant alterations in LAMP2 expression and the increased LAMP2 signal previously

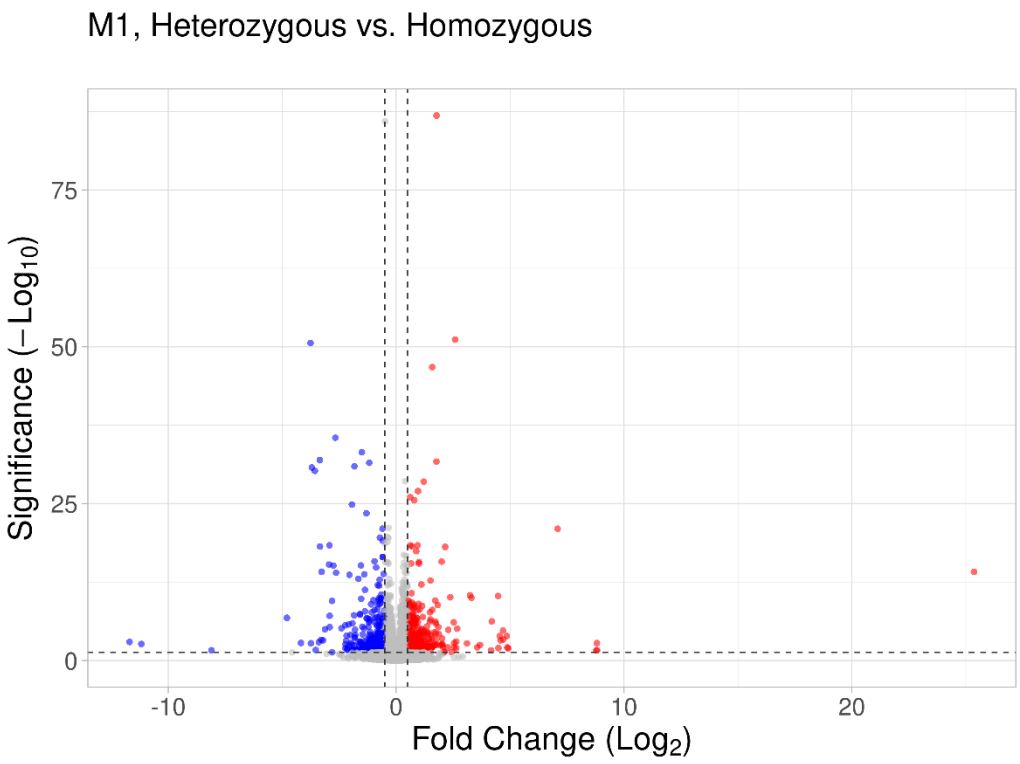

Figure 21- Volcano plot of heterozygous versus homozygous for M1 samples. The red dots represent upregulated genes, the blue ones represent down-regulated genes, and the gray ones are either not affected or no significance. Volcano plot was obtained with VolcaNoseR (Goedhart and Luijsterburg, 2020).

shown is not a result of increased protein synthesis. Rather, this is likely the result of impaired lysosomal trafficking and recycling that leads to its accumulation in the cytoplasm. Similar findings have already been reported by other studies focused on lysosomal homeostasis in NPC1. (Colaco et al., 2020) On another hand, we do see a downregulation of NPC1 protein, consistent with immunostaining results.

In M1 samples (figure 21) we do not observe upregulation of any of previously mentioned genes, which is in line with the PCA plot. All samples in M1 group cluster

together and only a total of 560 genes were found to be differentially expressed from which, 280 were up-regulated and another 280 genes were down-regulated.

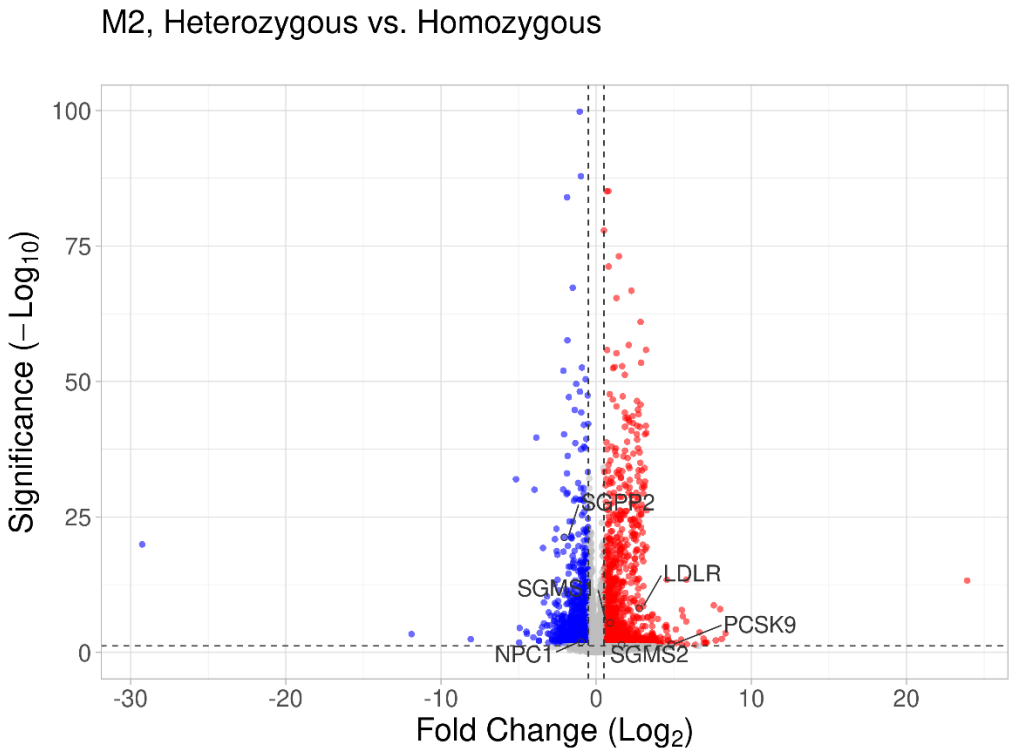

Figure 22- Volcano plot of heterozygous versus homozygous for M2 samples. The red dots represent up-regulated genes, the blue ones represent down-regulated genes, and the gray ones are either not affected or no significance. Volcano plot was obtained with VolcaNoseR (Goedhart and Luijsterburg, 2020).

On the other hand, M2 group (figure 22) presented the most differences between homozygous and heterozygous samples which, once again, corroborates the observations from the PCA plot. There, the groups are segregated, presenting the most DEGs with a total of 2031 from which, 1206 genes were up-regulated and 825 genes down-regulated. Moreover, M2 comparison not only presented SGPP2, SGMS1, and NPC1 as differentially expressed, but also SGMS2, LDLR (LDL Receptor) and PCSK9 (Proprotein convertase subtilisin/kexin type-9).

LDLR and PCSK9 are, in fact, closely connected. PCSK9 regulates LDL levels by mediating LDLR protein degradation by direct binding to it. This reaction has higher affinity at acidic pH, indicating a possible relevant role in the lysosomes (Joo Kwon et al., 2008). Regarding LDLR, we observe a significant up-regulation. This wasn't surprising since as mentioned before, sequestration of cholesterol in LE/LY and consequent accumulation leads to scarcity in receiving organelles due to low availability of free

cholesterol. This leads to a lack of negative feedback control and a vicious cycle in which the cell tries to compensate the lack of available cholesterol ending up exacerbating its accumulation.

Contrary to our results, Ishbashi et al (2010) reported no differential expression of LDLR in liver macrophages from mice and observed a reduced expression of PCSK9 (Ishibashi et al., 2010). However, in another study carried out by Frolov et al. (2003) in NPC1 fibroblast, an increase in the expression of LRLR was reported, which is in accordance with our results (Frolov et al., 2003). Intriguingly, in our case there is statistically significant difference of the above selected genes only in M2 iMph. This is an indication that the activation stage of the macrophages plays a key role in the transcriptomic profile of the cells, clearly impacting the overall transcript landscape. Moreover, taking into consideration previous results suggesting a high similarity between M0 and M2 iMph, it is possible that the disease phenotype is more prominent under resting (or more anti-inflammatory) conditions rather than when the cells are subjected to a striking proinflammatory stimulus such as IFN-γ. In fact, another well-known LSD – Gaucher Disease – in which lipidic burden is also one of the main hallmarks, is characterized by the predominancy of M2 macrophages, also called Gaucher cells (Pandey and Grabowski, 2013). Hence, the importance of the macrophage inflammation status in the disease phenotype might be important and a factor to consider when modelling and studying the disease, as we see a change in the DEG according to their polarization status.

Chapter 5

Conclusion

5. Concluding remarks

The work developed in this internship fell under the Niemann-Pick disease type C project of the Cellular Models and Drug Development R&D group at CENTOGENE GmbH, which aimed to characterize the iPSC derived macrophage model for NPC1 developed by the group and support all experimental work.

Due to the rarity of patients, and therefore no interest from the pharmaceutical industry to develop a treatment, rare diseases end up being understudied, resulting in misdiagnosis, delayed diagnosis, and few options for good treatment. (“Orphanet: About Orphan Drugs” n.d.; Nguengang Wakap et al. 2020) At the moment, NPCD has only one EMA approved therapy, Miglustat, that only slightly slows the progression of the disease, urging for new and more effective therapies.

For that, more and better cellular disease models are needed to improve the probabilities of successful translation of drug candidates from preclinical studies into clinical success. Most established disease models are either derived from other species or immortalized cell lines which skews their biological relevance. iPSC technology revolutionized the disease modelling field as it allowed to obtain primary tissue cultures never generated before in high quantities, therefore creating patient-derived disease models with high biological significance.

To that end, an iPSC derived macrophage model of NPCD was developed.

The developed model presented key macrophage markers, CD14, CD45, CD68, CD163 and CD86 and had the capacity to perform phagocytosis, confirming cell identity and functionality. In regard to disease relevance, patient iMph presented key phenotypical characteristics such as low NPC1 protein intensity in comparison to carrier iMph, along with higher LAMP2 signal, an indicative of defective endocytic trafficking. Through filipin staining we were able to confirm the presence of the main disease hallmark - cholesterol accumulating. We showed that patient iMph present large perinuclear filipin positive vesicles with apparent co-localization with LAMP2 but not with perilipin-2 positive vesicles, therefore indicating lysosomal accumulation of unesterified cholesterol. Such findings not only demonstrate the robustness of this protocol in generating reliable macrophages allied with great cell yield but also support its validity as a novel model to study NPCD.

Through RNA sequencing, we were able to evaluate the polarization potential of iMph NPCD model. Induction of both polarization statuses (M1 and M2) led to a marked change in cellular morphology that is in accordance with literature reports. Such modifications, together with the observed up-regulation of key IFN-γ pathway modulators and characteristic M1 and M2 cytokines confirmed the ability of iMph to acquire different polarization states in response to external stimulus. Additionally, in opposition to M1, M2 inflammatory induction only caused a minor shift in typical anti-inflammatory associated pathways when compared with M0. Based on that we suggest that the generated naïve macrophages are closer to M2 or M2-like.

From the transcriptomic data we also performed an initial assessment of the impact of the polarization status on the differences between NPC1 homozygous and heterozygous lines. Interestingly, our results suggest that different stages of macrophage activation have significant influence on the DEG profile, with M2 presenting considerably more DEGs when comparing carrier with patient iMph than the lowest group, M1. Although a more in-depth analysis (that was out of the scope of this work) is required to identify potential disease targets, these results point out the importance of taking cells' inflammatory profile into consideration when modelling NPCD and, likely, other diseases.

In sum, the developed model presented key macrophage and phenotypic characteristics, susceptible of being polarized into both extremes M1 and M2 constituting a new and adequate platform to further study NPCD and applicable for drug discovery in a HT setting.

Chapter 6
Future Prospects

6. Future Prospects

For future work, it would be relevant to characterize macrophage precursor cells and optimize culture conditions such as the differentiation medium into a non-serum-dependent alternative. Further protocol optimization to allow cryopreservation would also be an important step towards the mitigation of batch differences. In terms of disease phenotype, the development of an assay to evaluate autophagic flux in macrophages can potentially serve as an additional read-out in HT compound screening for NPC.

Finally, a deep dive into the generated data from RNA sequencing can be used to study in-depth differences in NPC1 iMph transcriptional signature. Its combination with complementary omics data (ex. Metabolomics) can serve as fuel for AI based systems to identify potential drug targets. This, with the advantage of being able to study simultaneously the influence of the cell polarization status.

Other activities

During this internship, I was included in the NPCD project and supported all the laboratory activities of the project that go beyond the techniques and results mentioned throughout this report.

In that sense, not only was I responsible for the whole maintenance, from start to finish, of macrophages used in our project but was also able to work with several other types of cells (ex. fibroblasts, neuronal progenitor cells, astrocytes).

I managed a fibroblast culture with multiple mutations, performed experiments of different nature, as well as phenotype confirmation via immunocytochemistry in a HT microscope. My tasks also comprised sample preparation for mass spectrometry for biomarker measurement in collaboration with the R&D Biochemistry Department which involved cell viability DNA measurements as well.

I was also involved in tool-compound and drug testing assays in both macrophages and fibroblasts, which led me to learn how to work with pipetting robots for 386 well plates for HT experiments. Furthermore, I acquired experience in viral and mRNA transfection and helped to develop an autophagy assay to measure autophagy levels in different cell types.

References

About Us: The CENTOGENE Story Available at: https://www.centogene.com/about-us/why-choose-centogene [Accessed May 28, 2022].

Ackermann, M., Kempf, H., Hetzel, M., Hesse, C., Hashtchin, A. R., Brinkert, K., et al. (2018). Bioreactor-based mass production of human iPSC-derived macrophages enables immunotherapies against bacterial airway infections. *Nat Commun* 9, 5088–5101. doi: 10.1038/s41467-018-07570-7.

Babraham Bioinformatics - FastQC A Quality Control tool for High Throughput Sequence Data Available at: https://www.bioinformatics.babraham.ac.uk/projects/fastqc/ [Accessed July 12, 2022].

bcl2fastq Conversion Software Available at: https://support.illumina.com/sequencing/sequencing_software/bcl2fastq-conversion-software.html [Accessed July 12, 2022].

Benjaminit, Y., and Hochberg, Y. (1995). Controlling the False Discovery Rate: a Practical and Powerful Approach to Multiple Testing.

Blaner, W. S., O'Byrne, S. M., Wongsiriroj, N., Kluwe, J., D'Ambrosio, D. M., Jiang, H., et al. (2009). Hepatic stellate cell lipid droplets: A specialized lipid droplet for retinoid storage. *Biochim Biophys Acta Mol Cell Biol Lipids* 1791, 467–473. doi: 10.1016/j.bbalip.2008.11.001.

Borger, D. K., McMahon, B., Lal, T. R., Serra-Vinardell, J., Aflaki, E., and Sidransky, E. (2017). Induced pluripotent stem cell models of lysosomal storage disorders. *DMM Disease Models and Mechanisms* 10, 691–704. doi: 10.1242/dmm.029009.

Buchrieser, J., James, W., and Moore, M. D. (2017). Human Induced Pluripotent Stem Cell-Derived Macrophages Share Ontogeny with MYB-Independent Tissue-Resident Macrophages. *Stem Cell Reports* 8, 334–345. doi: 10.1016/j.stemcr.2016.12.020.

Cao, X., Yakala, G. K., van den Hil, F. E., Cochrane, A., Mummery, C. L., and Orlova, V. v. (2019). Differentiation and Functional Comparison of Monocytes and Macrophages from hiPSCs with Peripheral Blood Derivatives. *Stem Cell Reports* 12, 1282–1297. doi: 10.1016/j.stemcr.2019.05.003.

Chistiakov, D. A., Killingsworth, M. C., Myasoedova, V. A., Orekhov, A. N., and Bobryshev, Y. v. (2017). CD68/macrosialin: Not just a histochemical marker. *Laboratory Investigation* 97, 4–13. doi: 10.1038/labinvest.2016.116.

Colaco, A., Kaya, E., Adriaenssens, E., Davis, L. C., Zampieri, S., Fernández-Suárez, M. E., et al. (2020). Mechanistic convergence and shared therapeutic targets in Niemann-Pick disease. *J Inherit Metab Dis* 43, 574–585. doi: 10.1002/jimd.12191.

Colombo, A., Dinkel, L., Müller, S. A., Sebastian Monasor, L., Schifferer, M., Cantuti-Castelvetri, L., et al. (2021). Loss of NPC1 enhances phagocytic uptake and impairs lipid trafficking in microglia. *Nat Commun* 12, 1–20. doi: 10.1038/s41467-021-21428-5.

Cougnoux, A., Yerger, J. C., Fellmeth, M., Serra-Vinardell, J., Martin, K., Navid, F., et al. (2020). Single cell transcriptome analysis of niemann–pick disease, type c1 cerebella. *Int J Mol Sci* 21, 1–23. doi: 10.3390/ijms21155368.

Crisler, W. J., Eshleman, E. M., and Lenz, L. L. (2019). Ligand-induced IFNGR1 down-regulation calibrates myeloid cell IFNγ responsiveness. *Life Sci Alliance* 2, 1–13. doi: 10.26508/lsa.201900447.

Dai, S., Dulcey, A. E., Hu, X., Wassif, C. A., Porter, F. D., Austin, C. P., et al. (2017). Methyl-β-cyclodextrin restores impaired autophagy flux in Niemann-Pick C1-deficient cells through activation of AMPK. *Autophagy* 13, 1435–1451. doi: 10.1080/15548627.2017.1329081.

Dobin, A., Davis, C. A., Schlesinger, F., Drenkow, J., Zaleski, C., Jha, S., et al. (2013). STAR: Ultrafast universal RNA-seq aligner. *Bioinformatics* 29, 15–21. doi: 10.1093/bioinformatics/bts635.

Eskelinen, E. L. (2006). Roles of LAMP-1 and LAMP-2 in lysosome biogenesis and autophagy. *Mol Aspects Med* 27, 495–502. doi: 10.1016/j.mam.2006.08.005.

Fabriek, B. O., van Bruggen, R., Mei Deng, D., M Ligtenberg, A. J., Nazmi, K., Schornagel, K., et al. (2009). The macrophage scavenger receptor CD163 functions as an innate immune sensor for bacteria. *Blood* 113, 887–892. doi: 10.1182/blood-2008-07.

Fonseca, D. A., Amaral, I., Pinto, A. C., and Cotrim, M. D. (2019). Orphan drugs: major development challenges at the clinical stage. *Drug Discov Today* 24, 867–872. doi: 10.1016/j.drudis.2019.01.005.

Frolov, A., Zielinski, S. E., Crowley, J. R., Dudley-Rucker, N., Schaffer, J. E., and Ory, D. S. (2003). NPC1 and NPC2 regulate cellular cholesterol homeostasis through generation of low density lipoprotein cholesterol-derived oxysterols. *Journal of Biological Chemistry* 278, 25517–25525. doi: 10.1074/jbc.M302588200.

Funes, S. C., Rios, M., Escobar-Vera, J., and Kalergis, A. M. (2018). Implications of macrophage polarization in autoimmunity. *Immunology* 154, 186–195. doi: 10.1111/imm.12910.

Geberhiwot, T., Moro, A., Dardis, A., Ramaswami, U., Sirrs, S., Marfa, M. P., et al. (2018). Consensus clinical management guidelines for Niemann-Pick disease type C. *Orphanet J Rare Dis* 13. doi: 10.1186/s13023-018-0785-7.

Gerrick, K. Y., Gerrick, E. R., Gupta, A., Wheelan, S. J., Yegnasubramanian, S., and Jaffee, E. M. (2018). Transcriptional profiling identifies novel regulators of macrophage polarization. *PLoS One* 13, 1–19. doi: 10.1371/journal.pone.0208602.

GitHub - alexdobin/STAR: RNA-seq aligner Available at: https://github.com/alexdobin/STAR [Accessed July 12, 2022].

Gläser, A., Hammerl, F., Gräler, M. H., Coldewey, S. M., Völkner, C., Frech, M. J., et al. (2020). Identification of brain-specific treatment effects in NPC1 disease by focusing on cellular and molecular changes of sphingosine-1-phosphate metabolism. *Int J Mol Sci* 21, 1–31. doi: 10.3390/ijms21124502.

Goedhart, J., and Luijsterburg, M. S. (2020). VolcaNoseR is a web app for creating, exploring, labeling and sharing volcano plots. *Sci Rep* 10, 20560–20565. doi: 10.1038/s41598-020-76603-3.

Greenspan, P., Mayer, E. P., and Fowler, S. D. (1985). Nile Red: A Selective Fluorescent Stain for Intracellular Lipid Droplets. *J Cell Biol* 100, 965–973.

Gu, B. J., Sun, C., Fuller, S., Skarratt, K. K., Petrou, S., and Wiley, J. S. (2014). A quantitative method for measuring innate phagocytosis by human monocytes using real-time flow cytometry. *Cytometry Part A* 85, 313–321. doi: 10.1002/cyto.a.22400.

Gutbier, S., Wanke, F., Dahm, N., Rümmelin, A., Zimmermann, S., Christensen, K., et al. (2020). Large-scale production of human IPSC-derived macrophages for drug screening. *Int J Mol Sci* 21, 1–23. doi: 10.3390/ijms21134808.

Hale, C., Yeung, A., Goulding, D., Pickard, D., Alasoo, K., Powrie, F., et al. (2015). Induced pluripotent stem cell derived macrophages as a cellular system to study Salmonella and other pathogens. *PLoS One* 10, 1–20. doi: 10.1371/journal.pone.0124307.

Hannun, Y. A., and Obeid, L. M. (2018). Sphingolipids and their metabolism in physiology and disease. *Nat Rev Mol Cell Biol* 19, 175–191. doi: 10.1038/nrm.2017.107.

Horvath, P., Aulner, N., Bickle, M., Davies, A. M., Nery, E. del, Ebner, D., et al. (2016). Screening out irrelevant cell-based models of disease. *Nat Rev Drug Discov* 15, 751–769. doi: 10.1038/nrd.2016.175.

Hu, G., Su, Y., Kang, B. H., Fan, Z., Dong, T., Brown, D. R., et al. (2021). High-throughput phenotypic screen and transcriptional analysis identify new compounds and targets for macrophage reprogramming. *Nat Commun* 12, 773–787. doi: 10.1038/s41467-021-21066-x.

Hu, X., Chakravarty, S. D., and Ivashkiv, L. B. (2008). Regulation of interferon and Toll-like receptor signaling during macrophage activation by opposing feedforward and feedback inhibition mechanisms. *Immunol Rev* 226, 41–56. doi: 10.1111/j.1600-065X.2008.00707.x.

Hu, Y.-B., Dammer, E. B., Ren, R.-J., and Wang, G. (2015). The endosomal-lysosomal system: from acidification and cargo sorting to neurodegeneration. *Transl Neurodegener* 4, 1–10. doi: 10.1186/s40035-015-0041-1.

Huynh, K. K., Gershenzon, E., and Grinstein, S. (2008). Cholesterol accumulation by macrophages impairs phagosome maturation. *Journal of Biological Chemistry* 283, 35745–35755. doi: 10.1074/jbc.M806232200.

Ikonen, E., and Zhou, X. (2021). Cholesterol transport between cellular membranes: A balancing act between interconnected lipid fluxes. *Dev Cell* 56, 1430–1436. doi: 10.1016/j.devcel.2021.04.025.

Ishibashi, M., Masson, D., Westerterp, M., Wang, N., Sayers, S., Li, R., et al. (2010). Reduced VLDL clearance in Apoe-/- Npc1-/- mice is associated with increased Pcsk9 and Idol expression and decreased hepatic LDL-receptor levels. *J Lipid Res* 51, 2655–2663. doi: 10.1194/jlr.M006163.

Karagiannis, P., Takahashi, K., Saito, M., Yoshida, Y., Okita, K., Watanabe, A., et al. (2019). Induced pluripotent stem cells and their use in human models of disease and development. *Physiol Rev* 99, 79–114. doi: 10.1152/physrev.00039.2017.

Kwon, H. J., Lagace, T. A., McNutt, M. C., Horton, J. D., and Deisenhofer, J. (2008). Molecular basis for LDL receptor recognition by PCSK9. *Proceedings of the National Academy of Sciences* 105, 1820–1825. doi: 10.1073/pnas.0712064105.

Lacey, D. C., Achuthan, A., Fleetwood, A. J., Dinh, H., Roiniotis, J., Scholz, G. M., et al. (2012). Defining GM-CSF– and Macrophage-CSF–Dependent Macrophage Responses by In Vitro Models. *The Journal of Immunology* 188, 5752–5765. doi: 10.4049/jimmunol.1103426.

Lee, C. Z. W., Kozaki, T., and Ginhoux, F. (2018). Studying tissue macrophages in vitro: are iPSC-derived cells the answer? *Nat Rev Immunol* 18, 716–725. doi: 10.1038/s41577-018-0054-y.

Lee, K. Y. (2019). M1 and M2 polarization of macrophages: a mini-review. *Medical Biological Science and Engineering* 2, 1–5. doi: 10.30579/mbse.2019.2.1.1.

Lensch, M. W., and Mummery, C. L. (2013). From stealing fire to cellular reprogramming: A scientific history leading to the 2012 Nobel Prize. *Stem Cell Reports* 1, 5–17. doi: 10.1016/j.stemcr.2013.05.001.

Li, X., Wang, J., Coutavas, E., Shi, H., Hao, Q., and Blobel, G. (2016). Structure of human Niemann-Pick C1 protein. *Proc Natl Acad Sci U S A* 113, 8212–8217. doi: 10.1073/pnas.1607795113.

Liao, Y., Smyth, G. K., and Shi, W. (2014). FeatureCounts: An efficient general purpose program for assigning sequence reads to genomic features. *Bioinformatics* 30, 923–930. doi: 10.1093/bioinformatics/btt656.

Liedtke, M., Völkner, C., Hermann, A., and Frech, M. J. (2022). Impact of Organelle Transport Deficits on Mitophagy and Autophagy in Niemann–Pick Disease Type C. *Cells* 11, 1–24. doi: 10.3390/cells11030507.

Lim, W. F., Inoue-Yokoo, T., Tan, K. S., Lai, M. I., and Sugiyama, D. (2013). Hematopoietic cell differentiation from embryonic and induced pluripotent stem cells. *Stem Cell Res Ther* 4, 1–11. doi: 10.1186/scrt222.

Liu, G., David, B. T., Trawczynski, M., and Fessler, R. G. (2020). Advances in Pluripotent Stem Cells: History, Mechanisms, Technologies, and Applications. *Stem Cell Rev Rep* 16, 3–32. doi: 10.1007/s12015-019-09935-x.

Liu, T., Zhang, L., Joo, D., and Sun, S. C. (2017). NF-κB signaling in inflammation. *Signal Transduct Target Ther* 2, 1–9. doi: 10.1038/sigtrans.2017.23.

Lopez, M. E., Klein, A. D., Hong, J., Dimbil, U. J., and Scott, M. P. (2012). Neuronal and epithelial cell rescue resolves chronic systemic inflammation in the lipid storage disorder Niemann-Pick C. *Hum Mol Genet* 21, 2946–2960. doi: 10.1093/hmg/dds126.

Lopez-Yrigoyen, M., May, A., Ventura, T., Taylor, H., Fidanza, A., Cassetta, L., et al. (2020). Production and characterization of human macrophages from pluripotent stem cells. *Journal of Visualized Experiments* 2020, 1–9. doi: 10.3791/61038.

Love, M. I., Huber, W., and Anders, S. (2014). Moderated estimation of fold change and dispersion for RNA-seq data with DESeq2. *Genome Biol* 15, 1–21. doi: 10.1186/s13059-014-0550-8.

Lunov, O., Syrovets, T., Loos, C., Beil, J., Delacher, M., Tron, K., et al. (2011). Differential uptake of functionalized polystyrene nanoparticles by human macrophages and a monocytic cell line. *ACS Nano* 5, 1657–1669. doi: 10.1021/nn2000756.

Lyadova, I., Gerasimova, T., and Nenasheva, T. (2021). Macrophages Derived From Human Induced Pluripotent Stem Cells: The Diversity of Protocols, Future Prospects, and Outstanding Questions. *Front Cell Dev Biol* 9. doi: 10.3389/fcell.2021.640703.

Macías-Vidal, J., Gort, L., Lluch, M., Pineda, M., and Coll, M. J. (2009). Nonsense-mediated mRNA decay process in nine alleles of Niemann-Pick type C patients from Spain. *Mol Genet Metab* 97, 60–64. doi: 10.1016/j.ymgme.2009.01.007.

Maetzel, D., Sarkar, S., Wang, H., Abi-Mosleh, L., Xu, P., Cheng, A. W., et al. (2014). Genetic and chemical correction of cholesterol accumulation and impaired autophagy in hepatic and neural cells derived from niemann-pick type C patient-specific iPS cells. *Stem Cell Reports* 2, 866–880. doi: 10.1016/j.stemcr.2014.03.014.

Mantovani, A., Sica, A., Sozzani, S., Allavena, P., Vecchi, A., and Locati, M. (2004). The chemokine system in diverse forms of macrophage activation and polarization. *Trends Immunol* 25, 677–686. doi: 10.1016/j.it.2004.09.015.

Martinez, F. O., and Gordon, S. (2014). The M1 and M2 paradigm of macrophage activation: Time for reassessment. *F1000Prime Rep* 6, 1–13. doi: 10.12703/P6-13.

Martinez, F. O., Gordon, S., Locati, M., and Mantovani, A. (2006). Transcriptional Profiling of the Human Monocyte-to-Macrophage Differentiation and Polarization: New Molecules and Patterns of Gene Expression. *The Journal of Immunology* 177, 7303–7311. doi: 10.4049/jimmunol.177.10.7303.

Matencio, A., Navarro-Orcajada, S., González-Ramón, A., García-Carmona, F., and López-Nicolás, J. M. (2020). Recent advances in the treatment of Niemann pick disease type C: A mini-review. *Int J Pharm* 584, 1–4. doi: 10.1016/j.ijpharm.2020.119440.

McWhorter, F. Y., Wang, T., Nguyen, P., Chung, T., and Liu, W. F. (2013). Modulation of macrophage phenotype by cell shape. *Proc Natl Acad Sci U S A* 110, 17253–17258. doi: 10.1073/pnas.1308887110.

Mengel, E., Patterson, M. C., da Riol, R. M., del Toro, M., Deodato, F., Gautschi, M., et al. (2021). Efficacy and safety of arimoclomol in Niemann-Pick disease type C: Results from a double-blind, randomised, placebo-controlled, multinational phase 2/3 trial of a novel treatment. *J Inherit Metab Dis* 44, 1463–1480. doi: 10.1002/jimd.12428.

Miglustat Gen.Orph | European Medicines Agency Available at: https://www.ema.europa.eu/en/medicines/human/EPAR/miglustat-genorph [Accessed August 10, 2022].

Mosser, D. M., and Edwards, J. P. (2008). Exploring the full spectrum of macrophage activation. *Nat Rev Immunol* 8, 958–969. doi: 10.1038/nri2448.

Munn, C., Burton, S., Dickerson, S., Bakshy, K., Strouse, A., and Rajesh, D. (2021). Generation of cryopreserved macrophages from normal and genetically engineered human pluripotent stem cells for disease modelling. *PLoS One* 16, 1–26. doi: 10.1371/journal.pone.0250107.

Muralidhar, A., Borbon, I. A., Esharif, D. M., Ke, W., Manacheril, R., Daines, M., et al. (2011). Pulmonary function and pathology in hydroxypropyl-beta-cyclodextin-treated and untreated Npc1-/- mice. *Mol Genet Metab* 103, 142–147. doi: 10.1016/j.ymgme.2011.03.001.

Murray, P. J., Allen, J. E., Biswas, S. K., Fisher, E. A., Gilroy, D. W., Goerdt, S., et al. (2014). Macrophage Activation and Polarization: Nomenclature and Experimental Guidelines. *Immunity* 41, 14–20. doi: 10.1016/j.immuni.2014.06.008.

Nadjar, Y., and Vanier, M. T. (2018). Niemann-pick disease type c. *Neurometabolic Hereditary Diseases of Adults* 5, 121–146. doi: 10.1007/978-3-319-76148-0_6.

Newton, J., Milstien, S., and Spiegel, S. (2018). Niemann-Pick type C disease: The atypical sphingolipidosis. *Adv Biol Regul* 70, 82–88. doi: 10.1016/j.jbior.2018.08.001.

Newton, J., Palladino, E. N. D., Weigel, C., Maceyka, M., Gräler, M. H., Senkal, C. E., et al. (2020). Targeting defective sphingosine kinase 1 in Niemann–Pick type C

disease with an activator mitigates cholesterol accumulation. *Journal of Biological Chemistry* 295, 9121–9134. doi: 10.1074/jbc.ra120.012659.

Nguengang Wakap, S., Lambert, D. M., Olry, A., Rodwell, C., Gueydan, C., Lanneau, V., et al. (2020). Estimating cumulative point prevalence of rare diseases: analysis of the Orphanet database. *European Journal of Human Genetics* 28, 165–173. doi: 10.1038/s41431-019-0508-0.

Olzmann, J. A., and Carvalho, P. (2019). Dynamics and functions of lipid droplets. *Nat Rev Mol Cell Biol* 20, 137–155. doi: 10.1038/s41580-018-0085-z.

Onal, G., Kutlu, O., Gozuacik, D., and Dokmeci Emre, S. (2017). Lipid Droplets in Health and Disease. *Lipids Health Dis* 16, 1–15. doi: 10.1186/s12944-017-0521-7.

Ordoñez, M. P., and Steele, J. W. (2017). Modeling Niemann Pick type C1 using human embryonic and induced pluripotent stem cells. *Brain Res* 1656, 63–67. doi: 10.1016/j.brainres.2016.03.007.

Orekhov, A. N., Orekhova, V. A., Nikiforov, N. G., Myasoedova, V. A., Grechko, A. v., Romanenko, E. B., et al. (2019). Monocyte differentiation and macrophage polarization. *Vessel Plus* 3, 10–30. doi: 10.20517/2574-1209.2019.04.

Orphanet: About Orphanet Available at: https://www.orpha.net/consor/cgi-bin/Education_AboutOrphanet.php?lng=EN [Accessed May 28, 2022].

Orphanet: About rare diseases Available at: https://www.orpha.net/consor/cgi-bin/Education_AboutRareDiseases.php?lng=EN [Accessed May 28, 2022].

Pacheco, C. D., and Lieberman, A. P. (2008). The pathogenesis of Niemann-Pick type C disease: A role for autophagy? *Expert Rev Mol Med* 10, 1–14. doi: 10.1017/S146239940800080X.

Pallottini, V., and Pfrieger, F. W. (2020). Understanding and treating niemann–pick type c disease: Models matter. *Int J Mol Sci* 21, 1–37. doi: 10.3390/ijms21238979.

Pandey, M. K., and Grabowski, G. A. (2013). Immunological Cells and Functions in Gaucher Disease. *Crit Rev Oncog.*, 197–220.

Patterson, M. C., Clayton, P., Gissen, P., Anheim, M., Bauer, ; Peter, Bonnot, O., et al. (2017). Recommendations for the detection and diagnosis of Niemann-Pick disease type C. *Neurol Clin Pract* 7, 499–511.

Paul, D., Achouri, S., Yoon, Y. Z., Herre, J., Bryant, C. E., and Cicuta, P. (2013). Phagocytosis dynamics depends on target shape. *Biophys J* 105, 1143–1150. doi: 10.1016/j.bpj.2013.07.036.

Peake, K. B., and Vance, J. E. (2012). Normalization of cholesterol homeostasis by 2-hydroxypropyl-β- cyclodextrin in neurons and glia from Niemann-Pick C1 (NPC1)-deficient mice. *Journal of Biological Chemistry* 287, 9290–9298. doi: 10.1074/jbc.M111.326405.

Peter, F., Rost, S., Rolfs, A., and Frech, M. J. (2017). Activation of PKC triggers rescue of NPC1 patient specific iPSC derived glial cells from gliosis. *Orphanet J Rare Dis* 12, 1–14. doi: 10.1186/s13023-017-0697-y.

Picard Tools - By Broad Institute Available at: http://broadinstitute.github.io/picard/ [Accessed July 12, 2022].

Pineda, M., Walterfang, M., and Patterson, M. C. (2018). Miglustat in Niemann-Pick disease type C patients: a review. *Orphanet J Rare Dis* 13, 1–21. doi: 10.1186/s13023-018-0844-0.

Platt, F. M., d'Azzo, A., Davidson, B. L., Neufeld, E. F., and Tifft, C. J. (2018). Lysosomal storage diseases. *Nat Rev Dis Primers* 4, 1–25. doi: 10.1038/s41572-018-0025-4.

Pogue, R. E., Cavalcanti, D. P., Shanker, S., Andrade, R. v, Aguiar, L. R., de Carvalho, J. L., et al. (2017). Rare genetic diseases: update on diagnosis, treatment and online resources. *Drug Discov Today* 00, 1–9. doi: 10.1016/j.

Rare diseases Available at: https://ec.europa.eu/health/non-communicable-diseases/steering-group/rare-diseases_en [Accessed May 28, 2022].

Reid, P. C., Sugii, S., and Chang, T. Y. (2003). Trafficking defects in endogenously synthesized cholesterol in fibroblasts, macrophages, hepatocytes, and glial cells from Niemann-Pick type C1 mice. *J Lipid Res* 44, 1010–1019. doi: 10.1194/jlr.M300009-JLR200.

Rimkunas, V. M., Graham, M. J., Crooke, R. M., and Liscum, L. (2009). In Vivo Antisense Oligonucleotide Reduction of NPC1 Expression as a Novel Mouse Model for Niemann Pick Type C-Associated Liver Disease. *Hepatology* 47, 1504–1512.

Rivera, T., Zhao, Y., Ni, Y., and Wang, J. (2020). Human-Induced Pluripotent Stem Cell Culture Methods Under cGMP Conditions. *Curr Protoc Stem Cell Biol* 54, 1–21. doi: 10.1002/cpsc.117.

Rostam, H. M., Reynolds, P. M., Alexander, M. R., Gadegaard, N., and Ghaemmaghami, A. M. (2017). Image based Machine Learning for identification of macrophage subsets. *Sci Rep* 7, 3521–3533. doi: 10.1038/s41598-017-03780-z.

Sarkar, S., Carroll, B., Buganim, Y., Maetzel, D., Ng, A. H. M., Cassady, J. P., et al. (2013). Impaired autophagy in the lipid-storage disorder niemann-pick type c1 disease. *Cell Rep* 5, 1302–1315. doi: 10.1016/j.celrep.2013.10.042.

Shi, Y., Inoue, H., Wu, J. C., and Yamanaka, S. (2017). Induced pluripotent stem cell technology: A decade of progress. *Nat Rev Drug Discov* 16, 115–130. doi: 10.1038/nrd.2016.245.

Singh, R., Kaushik, S., Wang, Y., Xiang, Y., Novak, I., Komatsu, M., et al. (2009). Autophagy regulates lipid metabolism. *Nature* 458, 1131–1135. doi: 10.1038/nature07976.

Singhal, A., Krystofiak, E. S., Jerome, W. G., and Song, B. (2020). 2-Hydroxypropyl-gamma-cyclodextrin overcomes NPC1 deficiency by enhancing lysosome-ER association and autophagy. *Sci Rep* 10, 1–14. doi: 10.1038/s41598-020-65627-4.

Sitarska, D., and Ługowska, A. (2019). Laboratory diagnosis of the Niemann-Pick type C disease: an inherited neurodegenerative disorder of cholesterol metabolism. *Metab Brain Dis* 34, 1253–1260. doi: 10.1007/s11011-019-00445-w.

Tang, Y., Li, H., and Liu, J. P. (2010). Niemann-pick disease type C: From molecule to clinic. in *Clinical and Experimental Pharmacology and Physiology*, 132–140. doi: 10.1111/j.1440-1681.2009.05235.x.

The CENTOGENE Biodatabank Available at: https://www.centogene.com/about-us/biodatabank [Accessed May 28, 2022].

Trombetta, A. C., Soldano, S., Contini, P., Tomatis, V., Ruaro, B., Paolino, S., et al. (2018). A circulating cell population showing both M1 and M2 monocyte/macrophage surface markers characterizes systemic sclerosis patients with lung involvement. *Respir Res* 19, 1–12. doi: 10.1186/s12931-018-0891-z.

Ushach, I., and Zlotnik, A. (2016). Biological role of granulocyte macrophage colony-stimulating factor (GM-CSF) and macrophage colony-stimulating factor (M-CSF) on cells of the myeloid lineage. *J Leukoc Biol* 100, 481–489. doi: 10.1189/jlb.3ru0316-144r.

van Wilgenburg, B., Browne, C., Vowles, J., and Cowley, S. A. (2013). Efficient, Long Term Production of Monocyte-Derived Macrophages from Human Pluripotent Stem Cells under Partly-Defined and Fully-Defined Conditions. *PLoS One* 8, 1–18. doi: 10.1371/journal.pone.0071098.

Vanier, M. T. (2010). Niemann-Pick disease type C. *Vanier Orphanet Journal of Rare Diseases* 5, 1–18. Available at: http://www.ojrd.com/content/5/1/16.

Vanier, M. T. (2013). “Niemann-Pick diseases,” in *Handbook of Clinical Neurology* (Elsevier B.V.), 1717–1721. doi: 10.1016/B978-0-444-59565-2.00041-1.

Vanier, M. T., and Latour, P. (2015). Laboratory diagnosis of Niemann-Pick disease type C: The filipin staining test. *Methods Cell Biol* 126, 357–375. doi: 10.1016/bs.mcb.2014.10.028.

Vanier, M. T., Rodriguez-Lafrasse, C., Rousson, R., Gazzah, N., Juge, M.-C., Pentchev, P. G., et al. (1991). Type C Niemann-Pick disease: spectrum of phenotypic variation in disruption of intracellular LDL-derived cholesterol processing. *Biochim Biophys Acta* 1096, 328–337.

Vanier’, M. T., Wenger’, D. A., Comly], M. E., Rousson~, R., Brady, R. 0, and Pentchev’, P. G. (1988). Niemann-Pick disease group C: clinical variability and diagnosis based on defective cholesterol ester if ication A collaborative study on 70 patients. *Clin Genet* 3, 3–331.

Völkner, C., Liedtke, M., Hermann, A., and Frech, M. J. (2021a). Pluripotent stem cells for disease modeling and drug discovery in niemann-pick type c1. *Int J Mol Sci* 22, 1–30. doi: 10.3390/ijms22020710.

Völkner, C., Liedtke, M., Untucht, R., Hermann, A., and Frech, M. J. (2021b). Patient-specific iPSC-derived neural differentiated and hepatocyte-like cells, carrying the compound heterozygous mutation p.V1023sfs*15/p.G992R, present the “variant” biochemical phenotype of niemann-pick type C1 disease. *Int J Mol Sci* 22, 1–19. doi: 10.3390/ijms222212184.

Wang, Y., Liu, D., Chen, P., Koeffler, H. P., Tong, X., and Xie, D. (2008). Negative feedback regulation of IFN-γ pathway by IFN regulatory factor 2 in esophageal cancers. *Cancer Res* 68, 1136–1143. doi: 10.1158/0008-5472.CAN-07-5021.

Wheeler, S., and Sillence, D. J. (2020). Niemann–Pick type C disease: cellular pathology and pharmacotherapy. *J Neurochem* 153, 674–692. doi: 10.1111/jnc.14895.

Wiedemann, C., Kumar, A., Lang, A., and Ohlenschläger, O. (2020). Cysteines and Disulfide Bonds as Structure-Forming Units: Insights From Different Domains of Life and the Potential for Characterization by NMR. *Front Chem* 8, 1–8. doi: 10.3389/fchem.2020.00280.

Wilhelm, L. P., Voilquin, L., Kobayashi, T., Tomasetto, C., and Alpy, F. (2019). “Intracellular and plasma membrane cholesterol labeling and quantification using filipin and GFP-D4,” in *Methods in Molecular Biology* (Humana Press Inc.), 137–152. doi: 10.1007/978-1-4939-9136-5_11.

Wynn, T. A., Chawla, A., and Pollard, J. W. (2013). Macrophage biology in development, homeostasis and disease. *Nature* 496, 445–455. doi: 10.1038/nature12034.

Yu, X. H., Jiang, N., Yao, P. B., Zheng, X. L., Cayabyab, F. S., and Tang, C. K. (2014). NPC1, intracellular cholesterol trafficking and atherosclerosis. *Clinica Chimica Acta* 429, 69–75. doi: 10.1016/j.cca.2013.11.026.

Zhang, X., Li, Z., Liu, Y., and Gai, Z. (2020). Great expectations: Induced pluripotent stem cell technologies in neurodevelopmental impairments. *Int J Med Sci* 18, 459–473. doi: 10.7150/ijms.51842.

Zhou, D., Huang, C., Lin, Z., Zhan, S., Kong, L., Fang, C., et al. (2014). Macrophage polarization and function with emphasis on the evolving roles of coordinated regulation of cellular signaling pathways. *Cell Signal* 26, 192–197. doi: 10.1016/j.cellsig.2013.11.004.